Eur. Phys. J. B **54**, 525–549 (2006)
DOI: 10.1140/epjb/e2007-00021-y

THE EUROPEAN PHYSICAL JOURNAL B

Phase separation of bacterial colonies in a limit of high degradation

Analogy with Jupiter's great red spot

P.H. Chavanis[a]

Laboratoire de Physique Théorique, Université Paul Sabatier, 118 route de Narbonne, 31062 Toulouse Cedex 4, France

Received 23 April 2006 / Received in final form 25 October 2006
Published online 19 January 2007 –

Abstract. We discuss the structure of the equilibrium states of a regularized Keller-Segel model describing the chemotaxis of bacterial populations. We consider the limit of high degradation of the secreted chemical where analytical results can be obtained. Below a critical effective temperature, the system experiences a second order phase transition from a homogeneous phase to an inhomogeneous phase formed by two domains with uniform concentration separated by a thin interface (domain wall). We study the properties of the interface and determine the bifurcation between a circular shape (spot) and a rectangular shape (stripe) as a function of the control parameters. We show the analogy with the structure of Jupiter's great red spot which also consists in two phases with uniform potential vorticity separated by a thin annular jet.

PACS. 05.20.-y Classical statistical mechanics – 05.45.-a Nonlinear dynamics and chaos – 05.40.Jc Brownian motion – 87.10.+e General theory and mathematical aspects

1 Introduction

The name chemotaxis refers to the motion of organisms induced by chemical signals [1]. In some cases, the biological organisms (bacteria, amoebae, endothelial cells, ants...) secrete a substance (pheromone, smell, food,...) that has an attractive effect on the organisms themselves. Therefore, in addition to their diffusive motion, they move preferentially along the gradient of concentration of the chemical they secrete (chemotactic flux). When attraction prevails over diffusion, the chemotaxis can trigger a self-accelerating process until a point at which aggregation takes place. This is the case for the slime mold *Dictyostelium discoideum* and for the bacteria *Escherichia coli*. This is referred to as chemotactic collapse. A model of slime mold aggregation has been introduced by Patlak [2] and Keller and Segel [3] in the form of two coupled differential equations. A simplified version of this model has been extensively studied in the case where the degradation of the secreted chemical can be neglected and an immediate production is assumed [4]. In that case, the Keller-Segel equations become isomorphic to the Smoluchowski-Poisson system describing self-gravitating Brownian particles [5]. A detailed study of the Smoluchowski-Poisson system has been performed by Chavanis and Sire [6–15] in a recent series of papers. These results also apply to the chemotactic problem provided that we properly reinterpret the parameters (in particular, the mass M used in biology plays the same role as the inverse temperature T^{-1} used in gravity). In $d = 1$, there is no collapse (except at $T = 0$) and the evolution of the mass profile satisfies a Burgers equation. In $d = 2$, the system reaches a statistical equilibrium state for $T > T_c$ and undergoes a self-similar collapse for $T = T_c$ or a quasi self-similar collapse for $T < T_c$ leading ultimately to a Dirac peak. In $d \geq 3$, the system first undergoes a self-similar collapse leading to a finite time singularity (the density profile behaves like $\rho \propto r^{-2}$ at $t = t_{coll}$) followed by the formation of a Dirac peak in the post-collapse regime. Long-lived metastable gaseous states can also exist above a critical temperature T_c. Interestingly, most of these results have been obtained analytically. On the other hand, a vast number of rigorous results concerning the existence and unicity of the solutions of the Keller-Segel model and the conditions of blow-up have been obtained in the community of applied mathematics. We refer to the review of Horstmann [16] for a connection to the mathematical literature. A summary of the most physical results obtained for the Keller-Segel model and the Smoluchowski-Poisson system will be given in Section 5.

[a] e-mail: chavanis@irsamc.ups-tlse.fr

In this paper, we consider novel aspects of the Keller-Segel model. We first introduce a regularized model that prevents finite time-blow up and the formation of (unphysical) singularities like infinite density profiles and Dirac peaks. In this model, the local density of cells is bounded by a maximum value $\rho(\mathbf{r},t) \leq \sigma_0$ which takes into account finite size effects and filling factors. Indeed, since the cells have a finite size, they cannot be compressed indefinitely. Therefore, the Dirac peaks (singularities) are replaced by smooth density profiles (aggregates). With this regularization, there exists steady solutions (similar to the Fermi-Dirac distribution) for any value of the control parameter, contrary to the usual Keller-Segel model where blow up occurs above a critical mass when there is no steady state (in $d \geq 2$). In addition, we consider the limit of high degradation of the chemical. In that limit, the interaction between cells due to chemotaxis becomes short-ranged. We show that, for sufficiently small (effective) temperatures $T < T_c$, the system undergoes a second order phase transition from a homogeneous phase to an inhomogeneous phase. The bacteria organize in two domains with uniform density $\rho_\pm$ separated by a thin interface. The resulting structure is similar to a "domain wall" in phase ordering kinetics [17]. We study in detail the structure of the interface (profile, width, surface tension,...) and determine the conditions for the bifurcation between a circular shape (spot) and a rectangular shape (stripe) in a square domain. This study can be performed analytically in the limit of high degradation (our study is also exact in $d = 1$). The more physical case of a finite degradation rate will be treated numerically in another work.

In previous papers [5,15,18–22], we have found a number of analogies between the chemotactic problem and other systems of physical interest: self-gravitating systems, 2D vortices, Bose-Einstein condensation, Burgers dynamics, Cahn-Hilliard equations, generalized thermodynamics... As mentioned previously, the simplified Keller-Segel model [4] is isomorphic to the Smoluchowski-Poisson system describing self-gravitating Brownian particles [6]. In this analogy, the concentration of the chemical produced by the bacteria plays a role similar to the gravitational potential in astrophysical systems (they are both solutions of a Poisson equation) so that a number of analogies between biology and gravity can be developped [5]. In addition, the collapse of bacterial populations for $M > M_c$ or the collapse of self-gravitating Brownian particles for $T < T_c$ is by many respects similar to the Bose-Einstein condensation in phase space [19]. Finally, there exists some analogies between the chemotactic aggregation of bacteria and the formation of large-scale vortices in 2D turbulence [18,5]. In that case, the concentration of bacteria plays the role of the vorticity and the concentration of the chemical produced by the bacteria plays the role of the streamfunction. In two-dimensional hydrodynamics, the vorticity field which is solution of the 2D Euler equation can achieve a statistical equilibrium state (on the coarse-grained scale) as a result of turbulent mixing (violent relaxation) [21]. In the two-levels approximation, the equilibrium vorticity profile is given by a Fermi-Dirac-like distribution [23–26]. Interestingly, this is similar to the steady state of the regularized Keller-Segel model introduced in this paper. Furthermore, in the quasi-geostrophic (QG) approximation relevant to geophysical flows [27], the finite value of the Rossby deformation radius introduces a shielding of the interaction between vortices which is formally similar to the degradation of the chemical in the chemotactic problem. In particular, the degradation factor k (the square root of the ratio between the chemical decay coefficient and the chemical diffusion coefficient) plays the same role as the inverse of the deformation radius R^{-1} in geophysics. They control the distance over which the interaction is efficient. In the context of jovian vortices, Sommeria et al. [28] and Bouchet and Sommeria [29] have considered the limit of a small deformation radius $R \to 0$ to account for the annular jet structure of Jupiter's great red spot. As we shall see, this is similar to considering a limit of high degradation in the chemotactic problem. Therefore, many interesting results can be obtained by developing the analogies between these different topics.

The paper is organized as follows. In Section 2, we introduce a regularized Keller-Segel model of chemotactic aggregation. We first provide a phenomenological derivation of this model followed by a more kinetic approach. In Section 3, we study the equilibrium states of this model in a limit of high degradation. For $T < T_c$, we show that the solutions are formed by two phases in contact separated by an interface (the stability of the uniform phase is considered in Appendix A). In Sections 3.1–3.3, we develop a "domain wall" theory to study the properties of the interface and determine its main characteristics (profile, width, surface tension,...). Asymptotic behaviours of these expressions are obtained for $T \to T_c$ and $T \to 0$ in Sections 3.4 and 3.5. Analytical approximations of the wall profile are given in Sections 3.6 and 3.7 in the form of self-similar solutions. Other approximations are given in Section 3.8 using match asymptotics. In Section 3.9, we show that the curvature radius is constant so that, in two dimensions, the interface is either a line (stripe) or a circle (spot). These results can be obtained equivalently by minimizing the free energy functional associated with the regularized Keller-Segel model (see Sect. 3.10). In Section 3.11, we determine the phase diagram of the system and the range of control parameters (B,T) where the equilibrium state is a stripe or a spot (the parameter B is related to the total mass of the configuration). In Section 4, we develop the close analogy between our biological system and the jet structure of Jupiter's great red spot and other jovian vortices. Finally, in Section 5 we discuss the connection of our study with other works.

2 The regularized Keller-Segel model

2.1 The dynamical equations

The general Keller-Segel model [3] describing the chemotaxis of bacterial populations consists in two coupled

differential equations

$$\frac{\partial \rho}{\partial t} = \nabla \cdot (D_2 \nabla \rho) - \nabla \cdot (D_1 \nabla c), \tag{1}$$

$$\epsilon \frac{\partial c}{\partial t} = -k(c)c + f(c)\rho + D_c \Delta c, \tag{2}$$

that govern the evolution of the density of bacteria $\rho(\mathbf{r}, t)$ and the evolution of the secreted chemical $c(\mathbf{r}, t)$. The bacteria diffuse with a diffusion coefficient D_2 and they also move in a direction of a positive gradient of the chemical (chemotactic drift). The coefficient D_1 is a measure of the strength of the influence of the chemical gradient on the flow of bacteria. On the other hand, the chemical is produced by the bacteria with a rate $f(c)$ and is degraded with a rate $k(c)$. It also diffuses with a diffusion coefficient D_c. In the general Keller-Segel model, $D_1 = D_1(\rho, c)$ and $D_2 = D_2(\rho, c)$ can both depend on the concentration of the bacteria and of the chemical. This takes into account microscopic constraints, like close-packing effects, that can hinder the movement of bacteria.

A very much studied version of the Keller-Segel model is provided by the system of equations

$$\frac{\partial \rho}{\partial t} = \nabla \cdot (D \nabla \rho - \chi \rho \nabla c), \tag{3}$$

$$\epsilon \frac{\partial c}{\partial t} = D' \Delta c + a\rho - bc, \tag{4}$$

where the parameters are positive constants. Equation (3) can be viewed as a mean-field Fokker-Planck equation associated with a Langevin dynamics of the form

$$\frac{d\mathbf{r}}{dt} = \chi \nabla c + \sqrt{2D}\mathbf{R}(t), \tag{5}$$

where $\mathbf{R}(t)$ is a white noise and χ plays the role of a mobility. The Langevin equation describes a point organism performing a random walk biased in the direction of a drift velocity proportional to the local chemical gradient. This description is appropriate for an organism which measures the spatial gradient accross its body such as the amoeba *Dictyostelium discoideum*. By contrast, most bacteria employ a more complex temporal-sensing mechanism that needs to be modelled adequately. However, on a coarse scale, the Langevin dynamics can serve as a simple effective dynamics for the motion of individuals.

The stationary solution of equation (3) is given by

$$\rho = A e^{\frac{\chi}{D} c}. \tag{6}$$

This is similar to the Boltzmann distribution for a system in a potential $-c$. This suggests to introducing an effective temperature through the relation $T_{eff} = D/\chi$ which is similar to the Einstein relation. For $\epsilon = 0$, the system (3–4) monotonically decreases the Lyapunov functional

$$F = -\frac{1}{2}\int \rho c \, d\mathbf{r} + \frac{D}{\chi}\int \rho \ln \rho \, d\mathbf{r}, \tag{7}$$

which is similar to a free energy $F = E - T_{eff} S$ where $E = -\frac{1}{2}\int \rho c d\mathbf{r}$ is the energy of interaction and $S = -\int \rho \ln \rho d\mathbf{r}$ is the Boltzmann entropic functional[1]. One has $\dot{F} \leq 0$ which is similar to the proper version of the H-theorem in the canonical ensemble [30,31]. For $\epsilon \neq 0$, the Lyapunov functional is [32]:

$$F = \frac{1}{2a}\int \left[D'(\nabla c)^2 + bc^2\right] d\mathbf{r} - \int \rho c \, d\mathbf{r} + \frac{D}{\chi}\int \rho \ln \rho \, d\mathbf{r}. \tag{8}$$

We shall consider here a more general situation where the mobility and the diffusion coefficient in the Keller-Segel model can depend on the density of bacteria. In that case, equation (3) is replaced by

$$\frac{\partial \rho}{\partial t} = \nabla \cdot [\nabla (D(\rho)\rho) - \chi(\rho)\rho \nabla c]. \tag{9}$$

This can be viewed as a nonlinear mean-field Fokker-Planck equation [18]. It is associated with a Langevin equation of the form

$$\frac{d\mathbf{r}}{dt} = \chi(\rho)\nabla c + \sqrt{2D(\rho)}\mathbf{R}(t). \tag{10}$$

We define the functions h and g by

$$Dh(\rho) = \frac{d}{d\rho}(\rho D(\rho)), \tag{11}$$

$$\chi g(\rho) = \rho \chi(\rho), \tag{12}$$

where D and χ are positive coefficients. With these notations, equation (9) can be rewritten

$$\frac{\partial \rho}{\partial t} = \nabla \cdot [Dh(\rho)\nabla \rho - \chi g(\rho)\nabla c]. \tag{13}$$

Setting $\beta = 1/T_{eff} = \chi/D$, we obtain

$$\frac{\partial \rho}{\partial t} = \nabla \cdot [D\left(h(\rho)\nabla \rho - \beta g(\rho)\nabla c\right)]. \tag{14}$$

This type of nonlinear mean-field Fokker-Planck equations has been discussed in [18,33–35]. They are associated with generalized entropic functionals of the form

$$S = -\int C(\rho) \, d\mathbf{r}, \tag{15}$$

where $C(\rho)$ is a convex function defined by

$$C''(\rho) = \frac{h(\rho)}{g(\rho)}. \tag{16}$$

The Lyapunov functional associated to equation (14) is the free energy equation (7) or equation (8) where the Boltzmann entropy is replaced by the generalized entropy (15). On the other hand, the steady states of equation (14) are given by

$$C'(\rho) = \beta c - \alpha. \tag{17}$$

[1] Note that these analogies with thermodynamics take even more sense if we remark that the simplified Keller-Segel model with $\epsilon = b = 0$ is isomorphic to the Smoluchowski-Poisson system for self-gravitating Brownian particles [5].

Since C is convex, this equation can be reversed to give $\rho = F(-\beta c+\alpha)$ where $F(x) = (C')^{-1}(-x)$ is a decreasing function.

The Keller-Segel model (3–4) is known to exhibit blow-up solutions when the chemotactic attraction prevails over diffusion [11,16]. This reproduces the chemotactic aggregation of bacterial populations. In theory, the density can take arbitrarily large values and ultimately form a Dirac peak. In reality, this singular evolution is unphysical as we expect finite size effects and close-packing effects to become important when the system aggregates and becomes dense enough. We shall regularize the problem by introducing a sort of filling factor in the drift-diffusion equation (3). Thus, we take $h(\rho) = 1$ and $g(\rho) = \rho(1 - \rho/\sigma_0)$ in equation (14) so that equation (3) is replaced by

$$\frac{\partial \rho}{\partial t} = \nabla \cdot \left[D \left(\nabla \rho - \beta \rho (1 - \rho/\sigma_0) \nabla c \right) \right]. \qquad (18)$$

With this modification, the mobility is reduced when the density becomes high (i.e. when ρ approaches the value σ_0) and this prevents singularities to form. Indeed, it can be shown that the density remains always bounded: $\rho(\mathbf{r}, t) \leq \sigma_0$ for all t. This bound is similar to the Pauli exclusion principle in quantum mechanics, but it occurs here in physical space. The regularized drift-diffusion equation (18) was introduced phenomenologically in [5,18] to avoid infinite values of the density.

In the following, we shall take $\epsilon = 0$ for simplicity. This is valid in a limit of high diffusivity of the chemical [4,32]. Of course, the results that are valid at equilibrium are independent on this assumption. If we introduce the notations $k^2 = b/D'$ and $\lambda = a/D'$, we obtain the regularized Keller-Segel model

$$\frac{\partial \rho}{\partial t} = \nabla \cdot \left[D \left(\nabla \rho - \beta \rho (1 - \rho/\sigma_0) \nabla c \right) \right], \qquad (19)$$

$$\Delta c - k^2 c = -\lambda \rho. \qquad (20)$$

The distance over which chemotaxis is effective is controlled by the quantity k^{-1} which is equal to the square root of the ratio between the chemical diffusion coefficient D' and the chemical decay b. For $k \to 0$, we obtain a Poisson equation modelling a system with a long-range interaction. For finite values of k, the interaction is shielded on a typical distance k^{-1}. For $k \to +\infty$, the interaction between cells due to chemotaxis becomes short-ranged.

The stationary solution of equation (19) is given by

$$\rho = \frac{\sigma_0}{1 + e^{-\beta c + \alpha}}, \qquad (21)$$

which is similar to the Fermi-Dirac distribution in physical space. From this expression, we clearly have $\rho(\mathbf{r}) \leq \sigma_0$ at equilibrium. Furthermore, the Lyapunov functional can be written in the form of a free energy $F = E - T_{\mathit{eff}} S$ where

$$E = -\frac{1}{2} \int \rho c \, d\mathbf{r} = -\frac{1}{2\lambda} \int \left[(\nabla c)^2 + k^2 c^2 \right] d\mathbf{r}, \qquad (22)$$

is the energy of interaction and

$$S = -\sigma_0 \int \left\{ \frac{\rho}{\sigma_0} \ln \frac{\rho}{\sigma_0} + \left(1 - \frac{\rho}{\sigma_0} \right) \ln \left(1 - \frac{\rho}{\sigma_0} \right) \right\} d\mathbf{r}, \qquad (23)$$

is the Fermi-Dirac entropic functional in physical space. The distribution (21) extremizes the free energy at fixed mass. Indeed, writing the first order variations in the form $\delta F + \alpha T_{\mathit{eff}} \delta M = 0$ where α is a Lagrange multiplier, we recover equation (21). Furthermore, it can be shown that a stationary solution of equations (19, 20) is linearly stable if, and only if, it is a *minimum* of F at fixed mass [18]. These properties remain valid for the more general Fokker-Planck equations (14).

2.2 Phenomenological derivation of the model

In this section, we develop a connection between the chemotactic problem and thermodynamics. To that purpose, we introduce the entropic functional (23) from a combinatorial analysis which respects an exclusion principle in physical space. Then, we obtain the dynamical equation (19) from arguments similar to the linear thermodynamics of Onsager.

We divide the domain into a very large number of microcells with size h. We assume that the size h is of the order of the size of a particle so that a microcell is occupied either by 0 or 1 particle. This is how the exclusion principle is introduced in the problem. We shall now group these microcells into macrocells each of which contains many microcells but remains nevertheless small compared to the spatial extension of the whole system. We call ν the number of microcells in a macrocell. Consider the configuration $\{n_i\}$ where there are n_1 particles in the 1st macrocell, n_2 in the 2nd macrocell etc., each occupying one of the ν microcells with no cohabitation. The number of ways of assigning a microcell to the first element of a macrocell is ν, to the second $\nu - 1$ etc. Assuming that the particles are indistinguishable, the number of ways of assigning microcells to all n_i particles in a macrocell is thus

$$\frac{1}{n_i!} \times \frac{\nu!}{(\nu - n_i)!}. \qquad (24)$$

To obtain the number of microstates corresponding to the macrostate $\{n_i\}$ defined by the number of particles n_i in each macrocell (irrespective of their precise position in the cell), we need to take the product of terms such as (24) over all macrocells. Thus, the number of microstates corresponding to the macrostate $\{n_i\}$, which is proportional to the a priori probability of the state $\{n_i\}$, is

$$W(\{n_i\}) = \prod_i \frac{\nu!}{n_i!(\nu - n_i)!}. \qquad (25)$$

This is the Fermi-Dirac statistics which is applied here in physical space. As is customary, we define the entropy of the state $\{n_i\}$ by

$$S(\{n_i\}) = \ln W(\{n_i\}). \qquad (26)$$

It is convenient here to return to a representation in terms of the density in the ith macrocell

$$\rho_i = \rho(\mathbf{r}_i) = \frac{n_i\, m}{\nu h^d} = \frac{n_i \sigma_0}{\nu}, \tag{27}$$

where we have defined $\sigma_0 = m/h^d$, which represents the maximum value of ρ due to the exclusion constraint. Now, using the Stirling formula, we have

$$\ln W(\{n_i\}) \simeq \sum_i \nu(\ln\nu - 1) - \nu\biggl\{\frac{\rho_i}{\sigma_0}\biggl[\ln\biggl(\frac{\nu\rho_i}{\sigma_0}\biggr) - 1\biggr] + \biggl(1-\frac{\rho_i}{\sigma_0}\biggr)\biggl[\ln\biggl\{\nu\biggl(1-\frac{\rho_i}{\sigma_0}\biggr)\biggr\} - 1\biggr]\biggr\}. \tag{28}$$

Passing to the continuum limit $\nu \to 0$, we obtain the expression (23) of the Fermi-Dirac entropy in physical space. In the dilute limit $\rho \ll \sigma_0$, it reduces to the Boltzmann entropy appearing in equation (7).

The entropy is the correct thermodynamical potential for an isolated system for which the energy is conserved (microcanonical ensemble). This is not the case for our system which is dissipative. The proper description is the canonical ensemble and the correct thermodynamical potential is the free energy $F = E - T_{\mathit{eff}} S$ constructed with the Fermi-Dirac entropy (23) and the energy (22). The equilibrium state in the canonical ensemble is obtained by minimizing the free energy at fixed mass. Writing the first variations as $\delta F - \lambda \delta M = 0$, we obtain

$$\frac{\delta F}{\delta\rho} - \lambda = 0, \tag{29}$$

which leads to the Fermi-Dirac distribution (21) with $\alpha = -\lambda\beta$. Now that the proper thermodynamical potential has been derived by a combinatorial analysis, we can introduce phenomenologically a dynamical model by writing the evolution of the density as a continuity equation $\partial_t\rho = \nabla\cdot\mathbf{J}$ where the current is the gradient of the functional derivative of the free energy, i.e.

$$\frac{\partial\rho}{\partial t} = \nabla\cdot\biggl(\mu\nabla\frac{\delta F}{\delta\rho}\biggr). \tag{30}$$

This formulation ensures that the free energy decreases monotonically provided that $\mu \geq 0$. Indeed,

$$\dot{F} = \int \frac{\delta F}{\delta\rho}\frac{\partial\rho}{\partial t}\, d\mathbf{r} = \int \frac{\delta F}{\delta\rho}\nabla\cdot\mathbf{J}\, d\mathbf{r} = -\int \mathbf{J}\cdot\nabla\frac{\delta F}{\delta\rho}\, d\mathbf{r} = -\int \mu\left(\nabla\frac{\delta F}{\delta\rho}\right)^2 d\mathbf{r} \leq 0. \tag{31}$$

Furthermore, a steady state satisfies $\dot{F} = 0$, i.e $\nabla(\delta F/\delta\rho) = 0$ leading to equation (29). Now, using equations (22) and (23), we have

$$\nabla\frac{\delta F}{\delta\rho} = -\nabla c + \frac{D}{\chi}\frac{\nabla\rho}{\rho(1-\rho/\sigma_0)}. \tag{32}$$

To avoid the singularity when $\rho = 0$ or $\rho = \sigma_0$, we require that μ is proportional to $\rho(1-\rho/\sigma_0)$. Writing equation (30) in the form

$$\frac{\partial\rho}{\partial t} = \nabla\cdot\biggl[\chi\rho(1-\rho/\sigma_0)\nabla\frac{\delta F}{\delta\rho}\biggr], \tag{33}$$

and using equation (32), we obtain equation (18). This approach to construct relaxation equations is equivalent to Onsager's linear thermodynamics. Indeed, noting that the potential

$$\lambda(\mathbf{r},t) \equiv \frac{\delta F}{\delta\rho} = -c + T_{\mathit{eff}}\ln\biggl(\frac{\rho/\sigma_0}{1-\rho/\sigma_0}\biggr), \tag{34}$$

is uniform at equilibrium according to equation (21) or (29), the linear thermodynamics of Onsager suggests to writing the current as

$$\mathbf{J} = \mu\nabla\lambda(\mathbf{r},t), \tag{35}$$

which is equivalent to equation (30). The same results can be obtained by a variational formulation which is related to the Maximum Entropy Production Principle (MEPP) [18]. The rate of dissipation of free energy is given by

$$\dot{F} = \int \frac{\delta F}{\delta\rho}\frac{\partial\rho}{\partial t}\, d\mathbf{r} = \int \frac{\delta F}{\delta\rho}\nabla\cdot\mathbf{J}\, d\mathbf{r} = -\int \mathbf{J}\cdot\nabla\frac{\delta F}{\delta\rho}\, d\mathbf{r}. \tag{36}$$

We shall determine the optimal current $\mathbf{J}_*$ which maximizes the rate of dissipation of free energy $\dot{F}$ under the constraint $J^2 \leq C(\mathbf{r},t)$ putting a (physical) bound on $|\mathbf{J}|$. The corresponding variational problem can be written

$$\delta\dot{F} + \delta\int\frac{\mathbf{J}^2}{2\mu}\, d\mathbf{r} = 0, \tag{37}$$

where μ is a Lagrange multiplier. Performing the variations on $\mathbf{J}$, we obtain $\mathbf{J}_* = \mu\nabla(\delta F/\delta\rho)$ which returns equation (30).

2.3 Kinetic derivation of the model

As discussed previously, equation (14) can be viewed as a nonlinear Fokker-Planck equation where the diffusion coefficient and the mobility explicitly depend on the local concentration of particles. Such generalized Fokker-Planck equations can be derived from a kinetic theory, starting from the master equation, and assuming that the probabilities of transition explicitly depend on the occupation number (concentration) of the initial and arrival states. Below, we briefly summarize and adapt to the present situation the approach developed by Kaniadakis [36] in a more general context.

We introduce a stochastic dynamics by defining the probability of transition of a bacteria from position $\mathbf{r}$ to position $\mathbf{r}'$. Following Kaniadakis [36], we assume the following form

$$\pi(\mathbf{r}\to\mathbf{r}') = w(\mathbf{r},\mathbf{r}-\mathbf{r}')a[\rho(\mathbf{r},t)]b[\rho(\mathbf{r}',t)]. \tag{38}$$

Usual stochastic processes correspond to $a(\rho) = \rho$ and $b(\rho) = 1$: the probability of transition is proportional to the density of the initial state and independent on the density of the final state. They lead to the Fokker-Planck equation (3) as will be shown below. Here, we assume a more general dependence on the occupancy in the initial and arrival states. This can account for microscopic constraints like close-packing effects that can inhibitate the transition. Quite generally, the evolution of the density satisfies the master equation

$$\frac{\partial \rho}{\partial t} = \int \left[\pi(\mathbf{r}' \to \mathbf{r}) - \pi(\mathbf{r} \to \mathbf{r}')\right] d\mathbf{r}'. \tag{39}$$

Assuming that the evolution is sufficiently slow, and local, such that the dynamics only permits values of $\mathbf{r}'$ close to $\mathbf{r}$, one can develop the term in brackets in equation (39) in powers of $\mathbf{r} - \mathbf{r}'$. Proceeding along the lines of [36], we obtain a Fokker-Planck-like equation

$$\frac{\partial \rho}{\partial t} = \frac{\partial}{\partial x_i}\left[\left(\zeta_i + \frac{\partial \zeta_{ij}}{\partial x_j}\right)\gamma(\rho) + \gamma(\rho)\frac{\partial \ln \kappa(\rho)}{\partial \rho}\zeta_{ij}\frac{\partial \rho}{\partial x_j}\right], \tag{40}$$

with

$$\gamma(\rho) = a(\rho)b(\rho), \qquad \kappa(\rho) = \frac{a(\rho)}{b(\rho)}, \tag{41}$$

and

$$\zeta_i(\mathbf{r}) = -\int y_i w(\mathbf{r}, \mathbf{y}) d\mathbf{y}, \tag{42}$$

$$\zeta_{ij}(\mathbf{r}) = \frac{1}{2}\int y_i y_j w(\mathbf{r}, \mathbf{y}) d\mathbf{y}. \tag{43}$$

The moments ζ_i and ζ_{ij} are fixed by the Langevin equation (5). Assuming isotropy

$$\zeta_i = J_i, \qquad \zeta_{ij} = D\delta_{ij}, \tag{44}$$

the kinetic equation becomes

$$\frac{\partial \rho}{\partial t} = \nabla \cdot \left[(\mathbf{J} + \nabla D)\gamma(\rho) + \gamma(\rho)\frac{\partial \ln \kappa(\rho)}{\partial \rho} D \nabla \rho\right]. \tag{45}$$

Now, according to the Langevin equation (5), D is independent on $\mathbf{r}$ and $\mathbf{J} = -\chi \nabla c$. Thus, we get

$$\frac{\partial \rho}{\partial t} = \nabla \cdot \left[D\gamma(\rho)\frac{\partial \ln \kappa(\rho)}{\partial \rho}\nabla \rho - \chi \gamma(\rho) \nabla c\right]. \tag{46}$$

If we define

$$h(\rho) = \gamma(\rho)\frac{\partial \ln \kappa(\rho)}{\partial \rho}, \qquad g(\rho) = \gamma(\rho), \tag{47}$$

the foregoing equation can be written

$$\frac{\partial \rho}{\partial t} = \nabla \cdot [Dh(\rho)\nabla \rho - \chi g(\rho) \nabla c], \tag{48}$$

and it coincides with the phenomenological equation (13). It seems natural to assume that the transition probability is proportional to the density of the initial state so that $a(\rho) = \rho$. In that case, we obtain an equation of the form

$$\frac{\partial \rho}{\partial t} = \nabla \cdot \left(D\left[b(\rho) - \rho b'(\rho)\right]\nabla \rho - \chi \rho b(\rho) \nabla c\right). \tag{49}$$

Note that the coefficients of diffusion and mobility are not independent since they are both expressed in terms of $b(\rho)$. Choosing $b(\rho) = 1$, i.e. a probability of transition which does not depend on the population of the arrival state, leads to the standard Fokker-Planck equation (3). If, now, we assume that the transition probability is blocked (inhibited) if the concentration of the arrival state is equal to σ_0, then it seems natural to take $b(\rho) = 1 - \rho/\sigma_0$. In that case, we obtain

$$\frac{\partial \rho}{\partial t} = \nabla \cdot (D\nabla \rho - \chi \rho(1 - \rho/\sigma_0)\nabla c), \tag{50}$$

which coincides with the phenomenological equation (18).

We can consider a related kinetic model with similar thermodynamical properties and the same equilibrium states. For this model, the dynamical equation reads

$$\frac{\partial \rho}{\partial t} = \nabla \cdot \left[\chi\left(\frac{T_{\mathit{eff}}}{1 - \rho/\sigma_0}\nabla \rho - \rho \nabla c\right)\right]. \tag{51}$$

This can be put in the form of a generalized Smoluchowski equation [18]:

$$\frac{\partial \rho}{\partial t} = \nabla \cdot \left[\frac{1}{\xi}\left(\nabla p - \rho \nabla c\right)\right], \tag{52}$$

associated with a barotropic equation of state $p(\rho) = -\sigma_0 T_{\mathit{eff}} \ln(1 - \rho/\sigma_0)$, where p is an effective "pressure". For $\rho \ll \sigma_0$, we recover the "isothermal" equation of state $p = \rho T_{\mathit{eff}}$ leading to the ordinary Keller-Segel model (3). However, for higher densities, the equation of state is modified. In particular, it prevents the density from exceeding the maximum value σ_0.

Equations (50) and (51) have very similar properties and they can be viewed as natural extensions of the Keller-Segel model. In equation (50) the regularization is put in the drift term (mobility) while in equation (51) it is put in the diffusion term (pressure). These two possibilities are considered in [18]. Note finally that equation (51) can be obtained from the master equation (39) when the transition probabilities are of the form (38) with $a(\rho) = \rho/\sqrt{1 - \rho/\sigma_0}$ and $b(\rho) = \sqrt{1 - \rho/\sigma_0}$.

3 Domain wall theory

3.1 The stationary state

The stationary solution of the regularized Keller-Segel model (19) is the Fermi-Dirac-like distribution

$$\rho = \frac{\sigma_0}{1 + e^{-\beta c + \alpha}}. \tag{53}$$

It relates, at equilibrium, the bacterial density ρ to the concentration of the chemical c. The chemical is itself produced by the bacteria according to equation (20). Thus, combining equations (53) and (20), we obtain a differential equation for the concentration c. Using the identity

$$\frac{1}{1+e^x}=\frac{1}{2}\left[1-\tanh\left(\frac{x}{2}\right)\right], \tag{54}$$

this mean-field equation can be written

$$\Delta c-k^2c=-\frac{\lambda\sigma_0}{2}\left[1-\tanh\left(\frac{\alpha-\beta c}{2}\right)\right]. \tag{55}$$

Introducing the new variables

$$\psi=\frac{c}{(\lambda\sigma_0/2)},\quad \mu=\frac{\alpha}{2},\quad C=\frac{\beta\lambda\sigma_0}{4k^2}, \tag{56}$$

we get

$$\Delta\psi-k^2\psi=-1+\tanh\left[C\left(\frac{\mu}{C}-k^2\psi\right)\right]. \tag{57}$$

In general, this equation must be solved numerically and different structures can be obtained depending on the values of the parameters. In order to gain some insight into the problem, we shall solve this equation perturbatively in a limit of high degradation of the chemical so that $k\gg 1$. In this limit of high decay, the communication distance between cells becomes very small. This limit is somewhat unrealistic for biological purposes since this prevents cells from efficiently communicating via chemotactic signals which is the aim of the whole process. However, this limit allows to obtain analytical results that may be representative of more physical regimes with finite degradation rate. Note also that the following treatment is exact in $1D$ without approximation. In the limit $k\to+\infty$, we can neglect the gradient of concentration except in a thin layer of width $\sim k^{-1}$ (domain wall) where the concentration changes rapidly. Outside the wall, we obtain the algebraic equation

$$-k^2\psi=-1+\tanh\left[C\left(\frac{\mu}{C}-k^2\psi\right)\right]. \tag{58}$$

In some range of parameters (see below), this equation determines two solutions $\psi_\pm$ which correspond to two phases with uniform concentration. These two phases are connected by a "wall". For $k\gg 1$, the interface is very thin so that we can neglect the curvature of the wall in a first approximation. The wall profile is then determined by the one-dimensional differential equation

$$\frac{d^2\psi}{d\xi^2}-k^2\psi=-1+\tanh\left[C\left(\frac{\mu}{C}-k^2\psi\right)\right], \tag{59}$$

where ξ is a coordinate normal to the interface.

3.2 The wall equation

If we set

$$\phi=k^2\psi-\mu/C,\quad \tau=k\xi,\quad \chi=\frac{\mu}{C}-1, \tag{60}$$

we obtain the wall equation

$$\frac{d^2\phi}{d\tau^2}=-\tanh(C\phi)+\phi+\chi. \tag{61}$$

Equation (61) is similar to the equation of motion for a particle in a potential

$$U(\phi)=T\ln\left[\cosh(\phi/T)\right]-\frac{\phi^2}{2}+\chi\phi+U_0, \tag{62}$$

where τ plays the role of time and ϕ plays the role of position. Indeed, it can be rewritten

$$\frac{d^2\phi}{d\tau^2}=-U'(\phi). \tag{63}$$

We have introduced the notation $C=1/T$ where, as we shall see, T plays the role of a temperature (it is furthermore proportional to the effective temperature T_{eff} defined previously). On the other hand, U_0 is a constant of integration that will be specified later.

Far from the wall, the density is uniform with values $\phi_\pm$ satisfying

$$U'(\phi_\pm)=0. \tag{64}$$

On the other hand, a conserved quantity of equation (63) is

$$E=\frac{1}{2}\left(\frac{d\phi}{d\tau}\right)^2+U(\phi). \tag{65}$$

The condition of solvability is therefore

$$U(\phi_-)=U(\phi_+). \tag{66}$$

The only possibility to satisfy the two conditions (64–66) simultaneously is that $\chi=0$, i.e $\mu=1/T$ (in that case, $U(\phi)$ is symmetric and the above conditions are satisfied trivially). Then, the wall profile is completely determined by the equations

$$\frac{d^2\phi}{d\tau^2}=-\tanh(\phi/T)+\phi, \tag{67}$$

$$U(\phi)=T\ln\left[\cosh(\phi/T)\right]-\frac{\phi^2}{2}+U_0, \tag{68}$$

$$\phi_\pm=\pm u,\qquad u=\tanh(u/T). \tag{69}$$

We note that the algebraic equation (69), equivalent to equation (64), has solutions $u\neq 0$ only if (see Fig. 1)

$$T<T_c=1. \tag{70}$$

This is similar to a second order phase transition (see Fig. 2). In that case, the algebraic equation has three solutions 0 and $\pm u$ with $u\leq 1$ (but the solution $\phi=u=0$ is unstable). The concentrations of bacteria and chemical in the uniform domains are related to the order parameter u by

$$c_\pm=\frac{\lambda\sigma_0}{2k^2}(1\pm u),\quad \rho_\pm=\frac{\sigma_0}{2}(1\pm u). \tag{71}$$

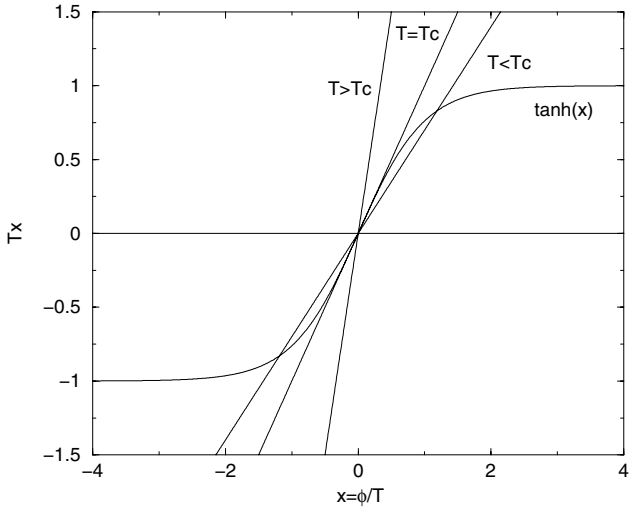

Fig. 1. Graphical construction determining the solutions $\pm u$ of the algebraic equation (69)-b as a function of the temperature T.

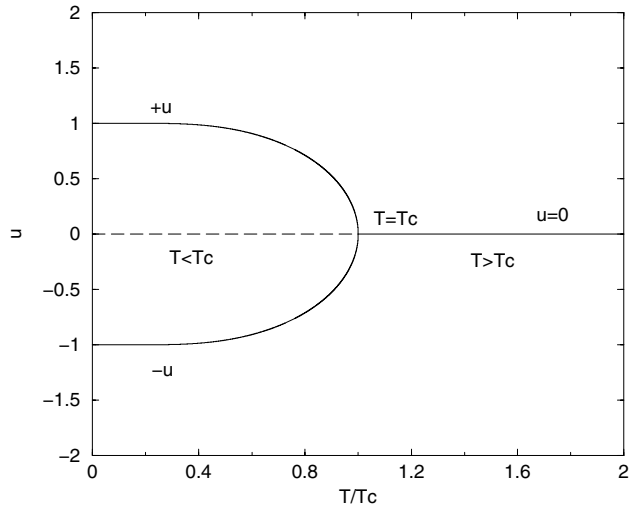

Fig. 2. Evolution of the order parameter u as a function of the temperature T. For $T > T_c$ the system is homogeneous with $\phi = u = 0$. For $T < T_c$, the uniform solution becomes unstable (see Appendix A) and two phases $\phi_\pm = \pm u$ separated by a "domain wall" appear.

More generally, using equations (53–54) the concentration profiles in the whole space can be expressed in terms of the field ϕ by

$$c = \frac{\lambda\sigma_0}{2k^2}(1+\phi), \quad \rho = \frac{\sigma_0}{2}\left[1+\tanh(\phi/T)\right]. \tag{72}$$

3.3 The wall profile

We determine U_0 such that $U(u) = 0$. The potential is then explicitly given by (see Fig. 3):

$$U(\phi) = T\ln\left[\cosh\left(\frac{\phi}{T}\right)\right] - \frac{\phi^2}{2} - T\ln\left[\cosh\left(\frac{u}{T}\right)\right] + \frac{u^2}{2}. \tag{73}$$

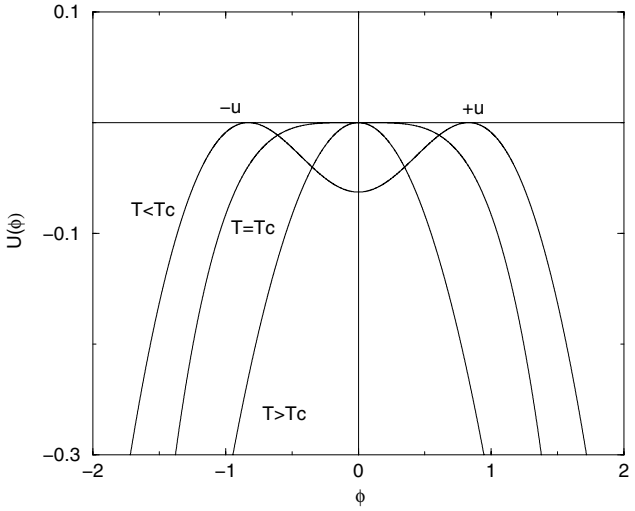

Fig. 3. The potential $U(\phi)$ of the equivalent mechanical problem for different values of the temperature.

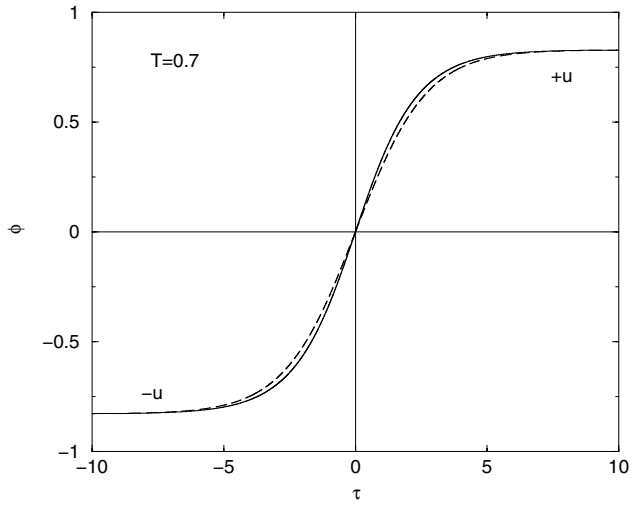

Fig. 4. Plot of the field ϕ accross the wall for $T = 0.7$. The solid line corresponds to the exact solution of equation (74) obtained numerically and the dashed line corresponds to the approximate expression (101).

With this convention, the constant appearing in equation (65) is $E = 0$. Then, we obtain the equation

$$\frac{1}{2}\left(\frac{d\phi}{d\tau}\right)^2 = -U(\phi), \tag{74}$$

which determines the wall profile by a simple integration (see Fig. 4)

$$\int_0^\phi \frac{dx}{\sqrt{-2U(x)}} = \tau. \tag{75}$$

For $\tau \to +\infty$, $\phi \to u$. To get the asymptotic behaviour, we set $\phi = u - \theta$ with $\theta \ll 1$ and we linearize the wall equation (74). This yields

$$\frac{d\theta}{d\tau} = -\sqrt{-U''(u)}\,\theta, \tag{76}$$

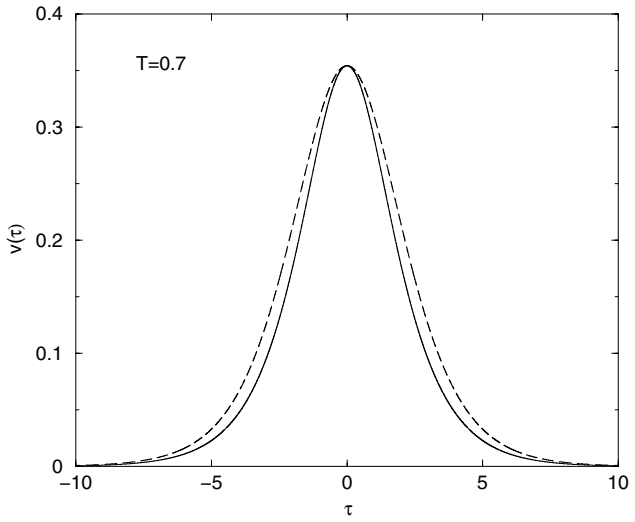

Fig. 5. Plot of the concentration gradient $v(\tau)$ accross the wall for $T = 0.7$. The solid line corresponds to the exact solution of equation (74) obtained numerically and the dashed line corresponds to the approximate expression (104–106).

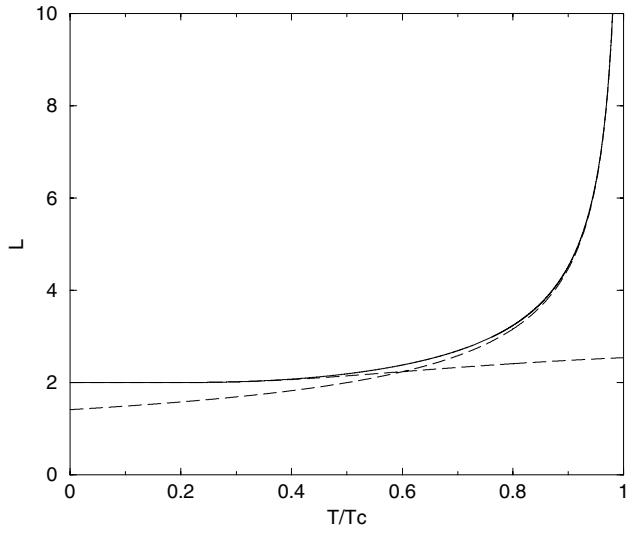

Fig. 6. Evolution of the typical width of the wall as a function of the temperature. The dashed lines correspond to the asymptotic expressions for $T \to 0$ and $T \to T_c$.

with $U''(u) = \frac{1}{T}(1-u^2) - 1 < 0$ for $T < T_c$. The wall connects the uniform phase exponentially rapidly. Thus, we can write

$$\phi = u - A(u)e^{-2\tau/L(u)}, \qquad (\tau \to +\infty) \tag{77}$$

where the typical width of the wall (expressed in units of k^{-1}) is

$$L(u) = \frac{2}{\sqrt{-U''(u)}} = \frac{2}{\sqrt{1-\frac{1}{T}(1-u^2)}}. \tag{78}$$

We introduce the concentration gradient (see Fig. 5)

$$v(\tau) = \frac{d\phi}{d\tau} = \sqrt{-2U(\phi)}. \tag{79}$$

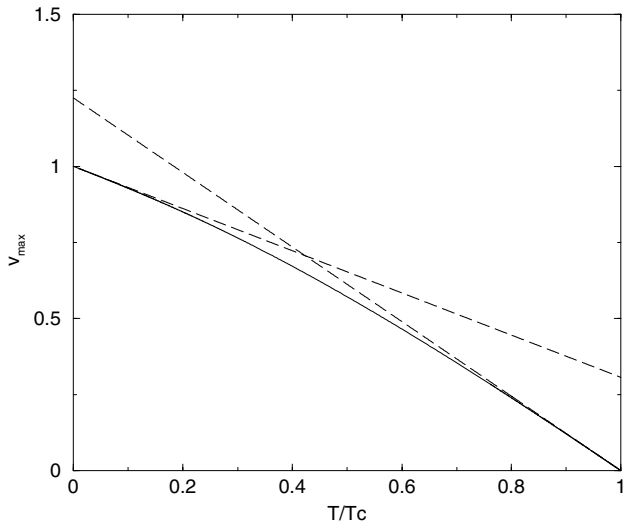

Fig. 7. Evolution of the maximum concentration gradient as a function of the temperature. The dashed lines correspond to the asymptotic expressions for $T \to 0$ and $T \to T_c$.

Using equation (73), we find that the maximum value of the concentration gradient, corresponding to $\phi = 0$, is given by

$$v_{max}(u) = \sqrt{2T\ln\left[\cosh\left(\frac{u}{T}\right)\right] - u^2}. \tag{80}$$

Finally, the energy of the wall, or surface tension, is

$$\sigma(u) = \int_{-\infty}^{+\infty}\left(\frac{d\phi}{d\tau}\right)^2 d\tau = \int_{-u}^{+u}\sqrt{-2U(\phi)}d\phi. \tag{81}$$

The functions L, v_{max} and σ are plotted in Figures 6–8 as a function of the temperature T, together with their asymptotic expressions computed in the following sections. The concentration profiles of bacteria and of the secreted chemical, given by equation (72), are plotted in Figure 9.

3.4 The limit $T \to T_c$

For $T \to T_c$, $u \to 0$ and $\phi \ll 1$. In that case, we can expand the potential to order ϕ^4 to obtain

$$U(\phi) = \frac{1}{2}(1-T)\phi^2 - \frac{1}{12}\phi^4 + U_0. \tag{82}$$

The wall equation becomes

$$\frac{d^2\phi}{d\tau^2} = -(1-T)\phi + \frac{1}{3}\phi^3. \tag{83}$$

The uniform solutions are $\phi = 0$ and $\phi^2 = 3(1-T)$ yielding

$$u = \sqrt{3(1-T)}. \tag{84}$$

We can now re-express the potential in the form

$$U(\phi) = -\frac{1}{12}(\phi^2 - u^2)^2. \tag{85}$$

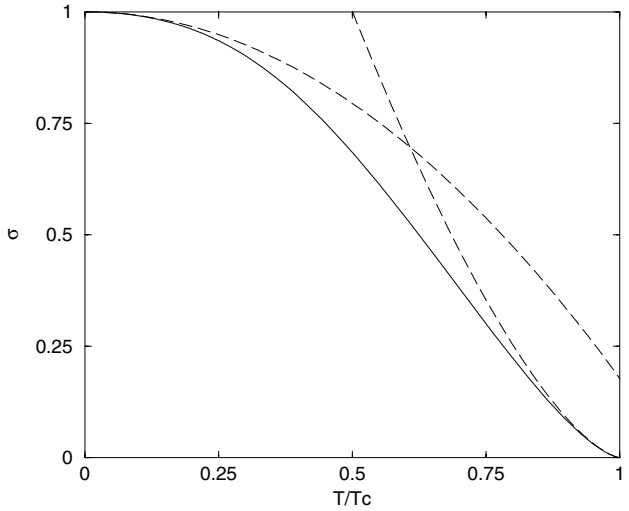

Fig. 8. Evolution of the energy of the wall (surface tension) as a function of the temperature. The dashed lines correspond to the asymptotic expressions for $T \to 0$ and $T \to T_c$.

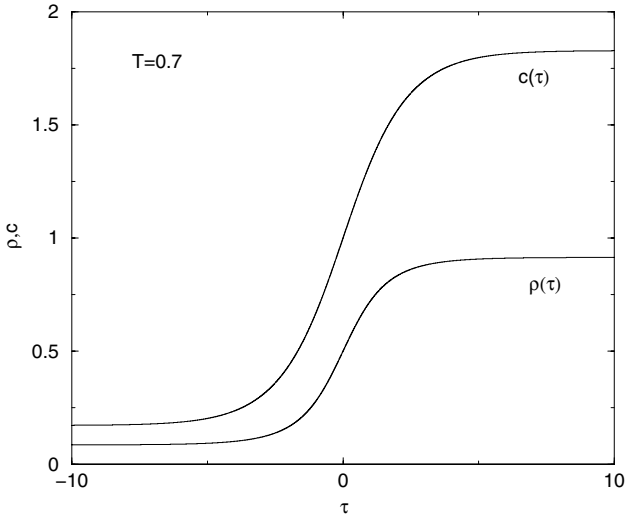

Fig. 9. Concentration profiles of bacteria ρ (in units of σ_0) and of the secreted chemical c (in units of $\lambda\sigma_0/2k^2$) for $T = 0.7$.

The wall profile (75) is given by

$$\int \frac{d\phi}{u^2 - \phi^2} = \frac{\tau}{\sqrt{6}}, \tag{86}$$

yielding explicitly

$$\phi = u \tanh\left(\frac{u\tau}{\sqrt{6}}\right). \tag{87}$$

The typical width of the wall, as defined by equation (78), is

$$L = \frac{\sqrt{6}}{u} = \sqrt{2}(1-T)^{-1/2}. \tag{88}$$

The width of the wall diverges at the critical point with the exponent $-1/2$. The wall profile can be rewritten

$$\phi = u(T) \tanh\left[\frac{\tau}{L(T)}\right], \tag{89}$$

and the concentration gradient is

$$v(\tau) = \frac{u(T)}{L(T)} \cosh^{-2}\left[\frac{\tau}{L(T)}\right]. \tag{90}$$

The maximum value of the concentration gradient is given by

$$v_{max} = \frac{u^2}{\sqrt{6}} = \left(\frac{3}{2}\right)^{1/2}(1-T), \tag{91}$$

and it tends to zero with the exponent $+1$ at the critical temperature. Finally, the surface tension is given by

$$\sigma = \left(\frac{2}{3}\right)^{3/2} u^3 = [2(1-T)]^{3/2}, \tag{92}$$

and it vanishes at the critical point with the exponent $+3/2$. These are the same scalings as in the classical Cahn-Hilliard theory [37].

3.5 The limit $T \to 0$

Setting $x = u/T$, equation (69)-b can be rewritten $Tx = \tanh(x)$. For $T \to 0$, $x \sim 1/T \to +\infty$ and $u \to 1$. More precisely, considering the behaviour of $\tanh(x)$ for $x \to +\infty$, we get

$$u \simeq 1 - 2e^{-2/T}. \tag{93}$$

The potential can be rewritten (for $\phi \geq 0$)

$$U(\phi) = \phi + Te^{-2\phi/T} - \frac{\phi^2}{2} + U_0. \tag{94}$$

The typical width of the wall is

$$L = 2\left(1 + \frac{2}{T}e^{-2/T}\right) = 2 - (1-u)\ln\left(\frac{1-u}{2}\right), \tag{95}$$

and the maximum value of the concentration gradient is

$$v_{max} = 1 - (\ln 2)T = 1 - \frac{2\ln 2}{\ln\left(\frac{1-u}{2}\right)}. \tag{96}$$

Finally, the surface tension is given by (see Appendix B)

$$\sigma = 1 - \frac{\pi^2}{12}T^2 = 1 - \frac{\pi^2}{6\ln\left(\frac{1-u}{2}\right)}. \tag{97}$$

For $T = 0$, we have $u = 1$ and

$$U(\phi) = \phi - \frac{\phi^2}{2} - \frac{1}{2} = -\frac{1}{2}(\phi - 1)^2. \tag{98}$$

The wall profile is solution of

$$\frac{d\phi}{d\tau} = 1 - \phi, \tag{99}$$

leading to

$$\phi = 1 - e^{-\tau} \qquad (\tau \geq 0). \tag{100}$$

3.6 Simple approximation for $T > 1/2$

If we are relatively close to the critical temperature $T_c = 1$, we can propose a simple approximation of the wall profile in the form

$$\phi = u(T)\tanh\left[\frac{\tau}{L(T)}\right], \tag{101}$$

where u and L are given by the *exact* expressions

$$u = \tanh\left(\frac{u}{T}\right), \tag{102}$$

$$L = \frac{2}{\sqrt{1-\frac{1}{T}(1-u^2)}}. \tag{103}$$

This Ansatz becomes exact when $T \to T_c$ and it provides a fair approximation for smaller temperatures (typically $T > 1/2$), see Figure 4.

The concentration gradient obtained from equation (101) is given by

$$v(\tau) = \frac{v_{max}(T)}{\cosh^2(\tau/L(T))}, \tag{104}$$

with the maximum value

$$v_{max} = \frac{u}{L} = \frac{u}{2}\sqrt{1-\frac{1}{T}(1-u^2)}. \tag{105}$$

However, it is more relevant to take for v_{max} the *exact* value (80), i.e.

$$v_{max} = \sqrt{2T\ln\left[\cosh\left(\frac{u}{T}\right)\right]-u^2}. \tag{106}$$

Typically, equation (104) with (105) gives a better agreement with the exact solution in the tail of profile while equation (104) with (105) gives a better agreement in the core of the profile, see Figure 5. Finally, the surface tension calculated with equation (104) is given by $\sigma = 4/3 v_{max}^2 L$.

3.7 Simple approximation for $T < 1/2$

For sufficiently small temperatures, we can propose a simple approximation of the wall profile in the form

$$\phi = u(T)\left[1-e^{-2\tau/L(u)}\right] \qquad (\tau \geq 0), \tag{107}$$

where u and L are given by the *exact* expressions (102) and (103). For $T = 0$, this Ansatz returns equation (100) and it provides a fair approximation of the exact profile for $T < 1/2$ (typically). The concentration gradient obtained from equation (107) is

$$v(\tau) = v_{max}(T)e^{-2|\tau|/L(T)}, \tag{108}$$

with the maximum value $v_{max} = 2u/L$. As before, it may be more relevant to use the exact value (106). The surface tension calculated with equation (108) is given by $\sigma = \frac{1}{2}v_{max}^2 L$ but this approximation yields an asymptotic behaviour for $T \to 0$ different from the exact result (97).

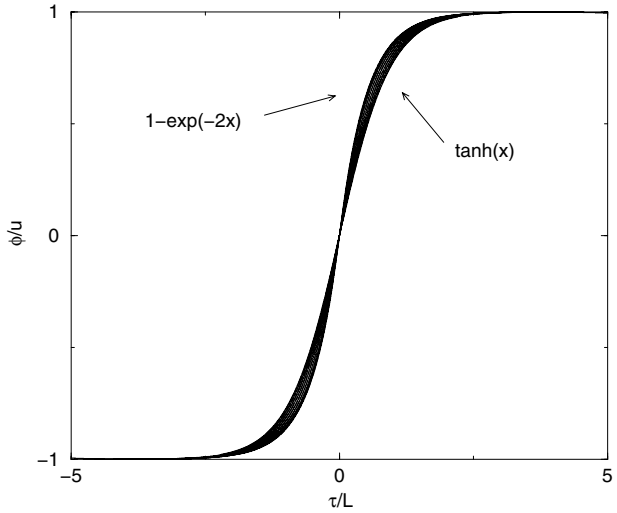

Fig. 10. Scaled concentration $\phi/u(T)$ as a function of the scaled distance $\tau/L(T)$ for different values of the temperature between $T = 0$ and $T = T_c = 1$. In terms of the scaled variables, the exact concentration profile is bounded by the solutions $1 - \exp(-2x)$ for $T = 0$ and $\tanh(x)$ for $T = T_c$.

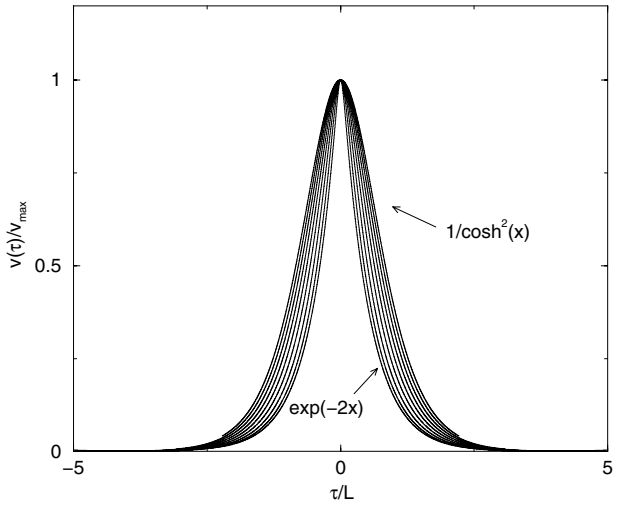

Fig. 11. Scaled concentration gradient $v/v_{max}(T)$ as a function of the scaled distance $\tau/L(T)$ for different values of the temperature between $T = 0$ and $T = T_c = 1$. In terms of the scaled variables, the exact profile of concentration gradient is bounded by the solutions $\exp(-2x)$ for $T = 0$ and $1/\cosh^2(x)$ for $T = T_c$.

The Ansatz (101) and (107) have a self-similar structure as a function of the temperature. Indeed, the functions $\phi(\tau)/u(T)$ and $v(\tau)/v_{max}(T)$ vs. $\tau/L(T)$ have an invariant profile. The exact solution of the differential equation (67) has not an exact self-similar structure as shown in Figures 10 and 11 but the region between the envelopes is relatively thin so that equations (101–107) can be useful approximations for $T \to 1$ and $T \to 0$ respectively. The profiles of concentration and concentration

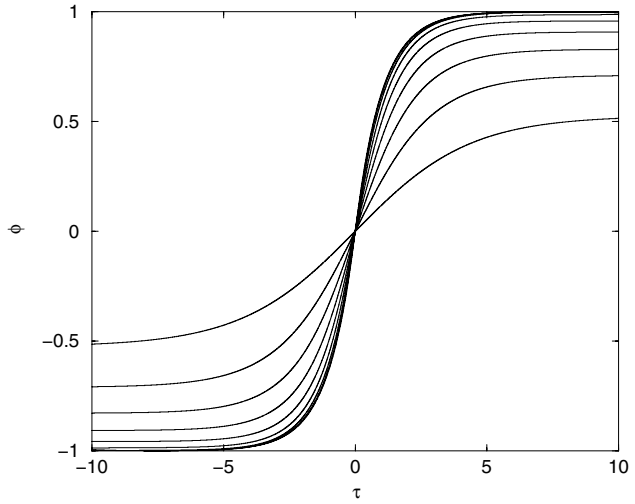

Fig. 12. Concentration ϕ as a function of the distance τ for different values of the temperature $T = 0.1$, 0.2, 0.3, 0.4, 0.5, 0.6, 0.7, 0.8 and 0.9.

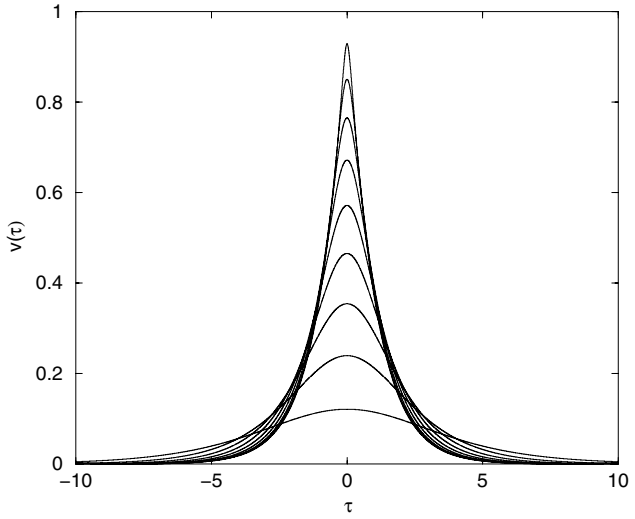

Fig. 13. Concentration gradient v as a function of the distance τ for different values of the temperature $T = 0.1$, 0.2, 0.3, 0.4, 0.5, 0.6, 0.7, 0.8 and 0.9.

gradient (in non-scaled variables) are plotted in Figures 12 and 13.

3.8 Match asymptotics

For small values of the temperature, one can propose another approximation of the profiles of concentration and concentration gradient by using match asymptotics.

3.8.1 Concentration profile $\phi(\tau)$

The exact asymptotic behaviours of the concentration profile are given by

$$\phi(\tau) \simeq v_{max}\tau + ... \qquad (\tau \to 0), \tag{109}$$

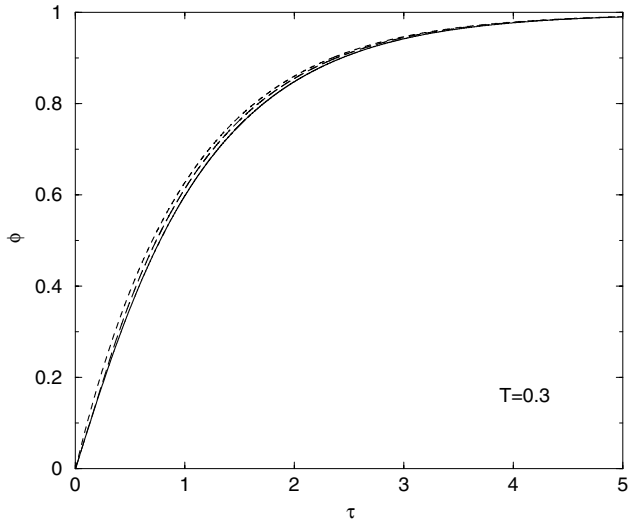

Fig. 14. Concentration profile for $T = 0.3$: exact (solid), approximate self-similar (dotted), match asymptotics (long-dashed).

$$\phi(\tau) = u - Ae^{-2\tau/L} \qquad (\tau \to +\infty), \tag{110}$$

where u, L and v_{max} are known functions of the temperature. We match these two behaviours at a point x where their values and the values of their first derivative coincide. This yields

$$x\, v_{max} = u - Ae^{-2x/L}, \tag{111}$$

$$v_{max} = \frac{2A}{L}e^{-2x/L}. \tag{112}$$

From these relations, we obtain

$$x = \frac{u}{v_{max}} - \frac{L}{2}, \tag{113}$$

$$A = \frac{L}{2}v_{max}e^{\frac{2u}{Lv_{max}}-1}. \tag{114}$$

For $T \to 0$, we explicitly find that

$$x = (\ln 2)T, \tag{115}$$

$$A = 1 - (\ln 2)^2T^2. \tag{116}$$

The exact concentration profile is plotted in Figure 14 for $T = 0.3$, and compared with the approximate self-similar expression (107) and the expression (109–110) obtained by match asymptotics.

3.8.2 Concentration gradient $\mathsf{v}(\tau)$

The exact asymptotic behaviours of the concentration gradient are given by

$$v(\tau) \simeq v_{max}\left[1 + \frac{1}{2}\left(1 - \frac{1}{T}\right)\tau^2 + ...\right] \quad (\tau \to 0), \tag{117}$$

$$v(\tau) = 2\frac{A}{L}e^{-2\tau/L} \qquad (\tau \to +\infty). \tag{118}$$

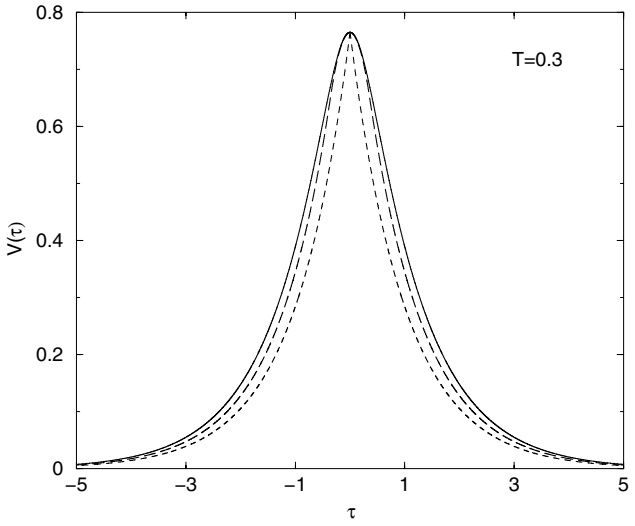

Fig. 15. Concentration gradient for $T = 0.3$: exact (solid), approximate self-similar (dotted), match asymptotics (long-dashed).

We match these two behaviours at a point x where their values and the values of their first derivative coincide. After simplification, we obtain

$$x = \frac{-L + \sqrt{L^2 + \frac{8T}{1-T}}}{2}, \tag{119}$$

$$A = \frac{L^2}{4} v_{max} \left(\frac{1}{T} - 1\right) x e^{2x/L}. \tag{120}$$

For $T \to 0$, we explicitly find that

$$x = T, \tag{121}$$

$$A = 1 + (1 - \ln 2)T. \tag{122}$$

The exact concentration gradient is plotted in Figure 15 for $T = 0.3$, and compared with the approximate self-similar expression (108–106) and the expression (117–118) obtained by match asymptotics.

3.9 The curvature radius

To next order in the expansion in $k^{-1} \ll 1$, we must account for the curvature of the interface. Close to the interface, $\nabla\psi = d\psi/d\xi \mathbf{n}$ where $\mathbf{n}$ is a unit vector normal to the wall. Introducing the curvature $r^{-1} = \nabla \cdot \mathbf{n}$ (r is the curvature radius), we get $\Delta\psi = d^2\psi/d\xi^2 + r^{-1} d\psi/d\xi$. Therefore, equation (57) becomes at first order

$$\frac{d^2\phi}{d\tau^2} + \frac{1}{kr}\frac{d\phi}{d\tau} = -U'(\phi) + \chi_1/k, \tag{123}$$

where we have written $\chi = \chi_0 + k^{-1}\chi_1 + ...$ and used the fact that $\chi_0 = 0$ at leading order (see Sect. 3.2). Multiplying equation (123) by $d\phi/d\tau$ and integrating across the wall we obtain the relation

$$\frac{1}{r} = -\frac{2\chi_1 u}{\sigma(u)}, \tag{124}$$

which shows that the radius of curvature r is constant. Therefore, the shape of the interface is either a circle (leading to a spot) or a straight line (leading to a stripe). Equation (124) is similar to Laplace's law relating the curvature radius of bubbles to the surface tension and to the difference of pressure between the interface (played here by $2u$).

3.10 The free energy

The previous results can be recovered by minimizing the 'free energy' (22–23) at fixed mass. This has been discussed in detail by Bouchet and Sommeria [29] in the context of jovian vortices where the problem is similar (see Sect. 4). Therefore, their study can be directly applied to the present situation and we shall only give the main steps of the analysis.

To leading order in $k^{-1} \to 0$, the system consists of two phases with uniform density $\rho_{\pm 1}$ and size $A_{\pm 1}$ (we call $A = A_+ + A_-$ the total size of the domain). Setting $\rho = \sigma_0/2(1+\phi)$ and $c = \lambda\sigma_0/2k^2(1+\phi)$, the free energy $F = E - T_{eff} S + \alpha T_{eff} M$ where E and S are given by equations (22–23) and M is the total mass can be written

$$F = A_1 f(\rho_1) + (A - A_1) f(\rho_{-1}), \tag{125}$$

with

$$f = \frac{T_{eff}\sigma_0}{2}[-C\phi^2 + (\alpha - 2C)\phi + (1+\phi)\ln(1+\phi) + (1-\phi)\ln(1-\phi)]. \tag{126}$$

The optimal values of $\rho_{\pm 1}$ and $A_{\pm 1}$ are obtained by minimizing the free energy (125). The variations on $\rho_{\pm 1}$ imply

$$f'(\rho_{\pm 1}) = 0, \qquad f''(\rho_{\pm 1}) > 0, \tag{127}$$

so that $\rho_\pm$ is a minimum of free energy. The variations on A_1 imply that

$$f(\rho_1) = f(\rho_{-1}). \tag{128}$$

This relation expresses the equality of the free energy of the two phases. The only possibility to satisfy the relations (127–128) simultaneously is to have $\alpha = 2C$ so that $f(\phi)$ is an odd function. This is equivalent to the solvability condition (66) leading to $\chi \equiv \alpha/2C - 1 = 0$. Then, it is straightforward to check that $f'(\rho) = 0$ implies that $\phi = \pm u$ where u is given by

$$Cu = \frac{1}{2}\ln\left(\frac{1+u}{1-u}\right) = \tanh^{-1}(u). \tag{129}$$

This returns the relation (69)-b.

To first order in k^{-1}, we need to determine the contribution of the free energy contained in the wall (interface). The free energy per unit length is given by

$$F_W = \frac{1}{k}\int_{-\infty}^{+\infty} [h(\rho(\tau)) - h(\rho_{\pm 1})]\, d\tau, \qquad (130)$$

where $h(\rho)$ is the density of free energy. Using equations (22, 23, 72) and (74), we obtain after simplification

$$F_W = \frac{\lambda\sigma_0^2}{4k^3}\int_{-\infty}^{+\infty} \left[\tilde{h}(\phi) - \tilde{h}(\phi_{\pm 1})\right] d\tau, \qquad (131)$$

with

$$\tilde{h}(\phi) = \phi(\tanh(C\phi) - \phi). \qquad (132)$$

Using $\tilde{h}(\phi_{\pm 1}) = \tilde{h}(u) = 0$ and $\tanh(C\phi) \geq \phi$ (see Fig. 1), we find that $F_W > 0$. Therefore, minimizing the free energy $F \sim lF_W$ amounts to minimizing the length l of the interface at fixed area. This gives either a circle or a straight line and this returns the fact that the curvature radius is constant (see Sect. 3.9). This argument also shows that it is more profitable to form, at equilibrium, a single "bubble" of size $A_\pm$ rather than several "droplets" of smaller size. However, a configuration with several "droplets" can exist as a non-equilibrium solution of the regularized Keller-Segel model (19–20). These droplets will evolve in time and merge together to finally form a single "bubble" (spot or stripe). This is similar to a coarsening process in spin systems [17] or to the aggregation of vortices in 2D decaying turbulence [38].

3.11 Bifurcations: spots and stripes

We shall work in a square domain with total size A. We consider periodic boundary conditions in order to avoid boundary effects. The equilibrium state consists in two phases with uniform density (ρ_+, A_+) and (ρ_-, A_-) with $A_+ + A_- = A$. We introduce the parameter

$$B = 1 - \frac{2M}{\sigma_0 A}. \qquad (133)$$

Since $0 \leq M \leq \sigma_0 A$, the parameter B takes values between -1 and $+1$. Writing $M = A_+\rho_+ + A_-\rho_-$ and using equation (71), the area of the two phases at equilibrium are given by

$$A_\pm = \frac{A}{2}\left(1 \mp \frac{B}{u}\right). \qquad (134)$$

They are determined by the parameter B (fixed by the total mass) and by the parameter u (fixed by the temperature). Since $0 \leq A_\pm \leq A$, we have the inequalities

$$|B| \leq u \leq 1, \qquad -1 \leq B \leq 1. \qquad (135)$$

Since the curvature radius is constant, we have three possible configurations: (i) a circular domain (spot) of phase + surrounded by phase −: the length of the interface is $2\sqrt{\pi A_+}$; (ii) a circular domain (spot) of phase − surrounded by phase +: in that case, the length of the interface is $2\sqrt{\pi(A - A_+)}$; (iii) a stripe of phase $\pm$ and a stripe of phase $\mp$: the length of the interface is $2\sqrt{A}$. The configuration selected at equilibrium is the one with the smallest interfacial length (see Fig. 16).

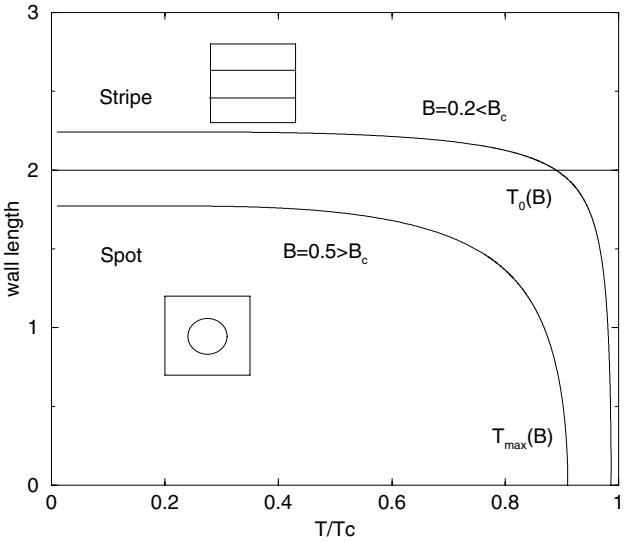

Fig. 16. Interfacial length of the spot (circle) as a function of the temperature for different values of the parameter B (the area of the domain has been normalized to $A = 1$). The spot is selected if its length is smaller than 2 and the stripe is selected in the other case. If $B > B_c = (\pi - 2)/\pi$, the spot is always selected. If $B < B_c$, the stripe is selected for $T < T_0(B)$ and the spot is selected for $T > T_0(B)$.

(i) The spot of phase + surrounded by phase − will be selected if $A_+ \leq A/\pi$, i.e. $u \leq \pi B/(\pi - 2)$. This is possible only for $B \geq 0$. In terms of the temperature, this corresponds to $T \geq T_0$ where $T_0(B)$ is determined by $u_0 = \tanh(u_0/T_0)$ with $u_0 = |B|\pi/(\pi - 2)$.

(ii) The circular domain of phase − surrounded by phase + will be selected if $A_+ \geq (1 - 1/\pi)A$, i.e. $u \leq -\pi B/(\pi - 2)$. This is possible only for $B \leq 0$. In terms of the temperature, this corresponds to $T \geq T_0$.

(iii) The stripes will be selected for $T < T_0$. This is possible only for $|B| \leq B_c \equiv (\pi - 2)/\pi$ (i.e. $u_0 \leq 1$). For $B > 0$, the stripe + has the smallest area ($A_+ \leq A_-$) and this is the opposite for $B < 0$.

Finally, we note that the condition $|B| \leq u$ implies that $T \leq T_{max}(B) \leq T_c$ where $T_{max}(B)$ is determined by $|B| = \tanh(|B|/T_{max})$.

The phase diagram is represented in Figure 17. This is the counterpart of the diagram obtained by Bouchet and Sommeria [29] for jovian vortices. The 'spots' are the equivalent of the 'vortices' and the 'stripes' are the equivalent of the 'jets'. The main difference (beyond the context and the interpretation of the solutions) is that the control parameter in our case is the effective temperature T

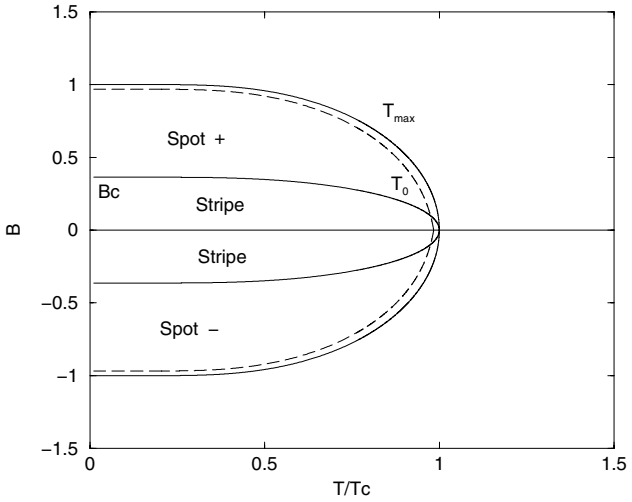

Fig. 17. Phase diagram of the regularized chemotactic model (19–20) showing the bifurcation between 'spots' and 'stripes' as a function of the control parameters (B, T). In a bounded domain, the solutions exist only for $T \leq T_{max}(B)$. We have drown the line of transition $T_0(B)$ between the two structures. Finally, the dashed line corresponds to the domain of validity of our perturbative expansion; it has been plotted for $Ak^2 = 1000$.

("canonical" situation) while their control parameter is the energy E (microcanonical situation).

Finally, concerning the domain of validity, our approach assumes that the domain size is larger than the interfacial width $L(u)/k$ given by equation (78) so that $A_{\pm} \geq (2L/k)^2$. This is satisfied on the left of the dashed line in Figure 17 corresponding to

$$|B| \leq u\left(1 - \frac{8L(u)^2}{Ak^2}\right). \tag{136}$$

4 Analogy with Jupiter's great red spot

4.1 The physical context

Vortices, waves and jets are ubiquitous in geophysical and astrophysical flows. Studying Jupiter's atmosphere is particularly rewarding because it presents many types of structures [39]: jet streams (belts and zones) flowing in straight lines eastward or westward and giving the planet a banded appearance, numerous long-lived anticyclones such as the Great Red Spot at 23S, the White Oval at 33S and the Little Red Spot at 19N, less common cyclones such as the elongated Brown Barges at 14N, a chain of 12 cyclones and 12 anticyclones at 41S (Karman vortex street), vortices presenting large amplitude east-west oscillations etc. In addition, Jupiter's cloud-top motions are easy to track from space providing detailed measurments for the upper circulation of the planet and for the velocity profiles of jets and vortices (several data are provided by the two Voyager encounters in 1979). Analogues of Jovian vortices have been reproduced in laboratory experiments [40–42] and in numerical simulations [43]. Long-lived vortices are also found in the atmosphere of other planets: Neptune's Great Dark Spot, Saturn's spot, Earth's atmospheric blocking highs, Gulf Stream rings, Mediterranean salt lens etc. These vortices are common features of rapidly rotating atmospheres and oceans and their robustness demands a general understanding. Because the convection is weak and the planet's rotation is strong, the horizontal motions are approximately 2D via the Taylor-Proudman theorem. Therefore, two-dimensional turbulence (possibly stratified) should be the proper framework to tackle the problem.

Jupiter's Great Red Spot (GRS) is probably the most famous example of vortex structures found in planetary atmospheres. The presence of this spot was first reported by Robert Hooke in 1664 in the first issue of the Philosophical Transaction of the Royal Society. The GRS is a large "eye" that dominates the southern hemisphere of the planet. It is an oval-shaped anticyclone with size 26 000 km by 13 000 km. Its breadth is about one hundred times its height so it can be considered approximately two-dimensional. It resides in a zonal shear at latitude 23S where the velocity changes sign, is elongated along the shear zone and is of the same sign as the background shear (these are relatively general rules observed for other vortices). It stays at the same latitude but slowly drifts in longitude. Morphologically, the GRS has a striking annular structure with a quiet center surrounded by a thin intense jet. The concentration of winds in an annulus is consistent with the fact that the GRS is much larger than the atmosphere's radius of deformation (the jet's width scales with the Rossby radius of deformation).

Since the GRS coexists with strong turbulence, its long-term stability can appear at first sights relatively surprising. Different theories of the Great Red Spot have been proposed over the years. The first hydrodynamic model for the GRS was proposed by Hide in 1963 who suggested that the spot could be a Taylor column on an isolated mountain. The variable drift of the GRS is in contradiction with this model. Also, there is now strong general astronomical and physical evidence that the giant planets are essentially fluid with only a relatively small solid core; hence Jovian spots must be free vortices. Maxworthy and Redekopp [44] examined the long wavelength limit of the Shallow-Water equations to obtain the KdV and modified KdV equations. They proposed that the GRS is a soliton solution of these equations in which the effects of phase dispersion and amplitude dispersion (nonlinearity) are in precise balance. However, this analytical model assumes that the structures are weakly nonlinear while the observed structures have a highly nonlinear behaviour. Another drawback of the soliton model is that it requires the radius of deformation to be of the same order as the spot width. In fact, the radius of deformation is about 500–2500 km, much smaller than the GRS. Therefore, this model does not account for the thin annular structure of the vortex nor does it reproduce the 2:1 elliptical shape of the GRS. Finally, the soliton theory predicts an interpenetration of vortices without change of structure while the real interaction between

vortices is a merging process. This is indeed a major property of 2D turbulence. Unlike in 3D turbulence where the energy cascades to smaller and smaller scales, in 2D the energy cascades to larger scales (inverse cascade) [45]. In other words, 2D vortices merge which explains the maintenance and robustness of large scale vortices. This point was recognized in particular by Ingersoll and Cuong [46] who argued that the GRS is Quasi-Geostrophic (QG) and maintains itself against dissipation by absorbing smaller vortices which are produced by convection.

A different point of view was advocated by Williams [47] and Antipov et al. [41] who independently proposed that the GRS is a solitary wave solution to the Intermediate Geostrophic (IG) equations. This solitary vortex can be obtained at scales much larger than the radius of deformation. In addition, their theory and experiments have the attractive property that anti-cyclones are prefered over cyclones while the QG model of Ingersoll and Cuong [46] does not make this seggregation. However, the IG model suffers from several drawbacks. First, it predicts that the vorticity of the GRS should be Gaussianly peaked at its center rather than in a circumpherential ring. In addition, IG theory predicts that the vortices move west at the local Rossby long-wave speed while QG theory and observations indicate that Jovian spots are advected by the background zonal flow. Marcus [43] argued that a permanent vortex can coexist with turbulence and that most of the properties of the Jovian vortices can be easily explained and understood with QG theory. In addition, he emphasized the jet structure of the GRS and showed that an annular jet is the natural structure of a vortex with a uniform potential vorticity inside and outside the spot. Marcus conducted numerical simulations in an anticyclonic annular shear. He observed that anticyclonic vorticity always formed robust anticyclonic vortices while cyclonic vortices were quickly stretched by the shear. The main conclusion of the work of Marcus is that the interaction of a vortex with turbulent eddies, rather than destroying the vortex feeds it by the merging process. Similar observations were made by Sommeria et al. [42] in laboratory experiments.

If the robustness of the GRS is due to a mixing process, it is natural to try to explain its structure and stability in terms of statistical mechanics. A statistical mechanics of two-dimensional vortices was first proposed by Onsager [48] in the point vortex model. He showed that the organization of point vortices in "macrovortices" occurs at negative temperatures. His ideas were further developed by Joyce and Montgomery [49] and Lundgren and Pointin [50] in a mean-field approximation. However, the physical applications of the point vortex model are limited. The statistical mechanics approach was extended by Kuz'min [51], Miller [24] and Robert and Sommeria [25] for continuous vorticity flows described by the 2D Euler equation. This theory predicts the organization of 2D turbulence into large-scale structures (jets and vortices) similar to those observed in the atmospheres and oceans. In particular, this theory is able to account for the "zoology" of vortices (monopoles, dipoles, tripoles,...) found in two-dimensional flows [52]. A similar statistical approach (theory of violent relaxation) was developed previously by Lynden-Bell [23] for the Vlasov equation to explain the structure of galaxies in the universe. The analogy between the statistical mechanics of 2D vortices and galaxies has been discussed and developed by Chavanis [21,26].

The possibility of using the statistical theory to explain the Great Red Spot was suggested at the start [24,25,53] but explicit predictions have been made only recently for a realistic model of the Jovian atmosphere proposed by Dowling and Ingersoll [54]. Sommeria et al. [28] extended the statistical theory to the QG model and investigated the limit of small Rossby radius. In that limit, PV mixing (entropic effects) with constraints on the energy leads to an equilibrium state that consists of two phases with uniform PV in contact separated by a strong jet. This precisely accounts for the morphology of the GRS and gives a theoretical justification to the model introduced phenomenologically by Marcus [43]. The statistical theory has been further developed by Bouchet and Sommeria [29] with quantitative applications to Jovian vortices. These authors interpreted the structure of the GRS as the coexistence of two thermodynamical phases in contact. The interface (jet) is determined by a problem of surface tension. The oval shape of the GRS is explained by the motion of the deep fluid which acts as an "effective topography". The position of the spot is shown to coincide with the extremum of topography (i.e. the latitude at which the shear vanishes) and the predicted velocity field agrees with the measurments of the Voyager missions. Small deviations in the initial parameters account for elongated structures similar to the Brown Barges or the intense jets observed in the north hemisphere. These results can be extended to the more physical Shallow-Water system [55,56]. Another model of Jupiter's great red spot has been proposed by Turkington et al. [57]. It predicts the emergence of a vortex solution at the correct latitude but does not reproduce the annular jet structure of the GRS [58].

4.2 Statistical mechanics of the quasi-geostrophic equations

The quasi-geostrophic equations appropriate to the dynamics of geophysical flows [27] can be written:

$$\frac{\partial q}{\partial t} + \mathbf{u} \cdot \nabla q = 0, \tag{137}$$

$$q = -\Delta\psi + \frac{\psi}{R^2} - Rh(y), \quad \mathbf{u} = -\hat{\mathbf{z}} \times \nabla\psi. \tag{138}$$

Here, q is the potential vorticity (PV) and ψ the stream function ($\hat{\mathbf{z}}$ is a unit vector normal to the two-dimensional flow). We have assumed that the topography $Rh(y)$ scales with the Rossby radius R. The QG equations admit an infinite number of stationary solutions specified by any relationship $q = f(\psi)$. Starting from an unstable initial condition, the flow undergoes a turbulent mixing and finally reaches a stationary state on the coarse-grained

scale. For given initial conditions, the statistical theory selects the *most probable state* consistent with the constraints imposed by the dynamics. It is obtained by maximizing a mixing entropy at fixed energy and Casimir constraints [24–26].

Let us consider the situation where the fine-grained PV q takes only two values $\{a_{-1}, a_1\}$. It is convenient to rescale the parameters so that $(a_1 - a_{-1})/2 = 1$ and $(a_1 + a_{-1})/2 = B$. We also choose the Gauge condition on ψ such that $\langle q\rangle = 0$ [29]. Then, the total area occupied by level a_1 is $\mathcal{A} = (1 - B)/2$ (the total area of the domain is unity). In the two-levels approximation [24–26], the mixing entropy is given by

$$S = -\int [p\ln p + (1-p)\ln(1-p)]d\mathbf{r}, \qquad (139)$$

where $p(\mathbf{r})$ is the local probability density of level a_1. The coarse-grained PV is $\overline{q} = pa_1 + (1-p)a_{-1}$. The extremization of (139) at fixed energy

$$E = \frac{1}{2}\int(\overline{q}+h)\psi d\mathbf{r} = \frac{1}{2}\int\left[(\nabla\psi)^2 + \frac{\psi^2}{R^2}\right]d\mathbf{r}, \quad (140)$$

and total patch area $\mathcal{A} = \int p(\mathbf{r})d\mathbf{r}$ leads to a $q-\psi$ relation of the form

$$\overline{q} = B - \tanh\left(\alpha - \frac{C\psi}{R^2}\right), \qquad (141)$$

where α and C are Lagrange multipliers introduced in the variational problem $\delta S - 2\alpha\delta\mathcal{A} + C/R^2\delta E = 0$.

Robert and Sommeria [59] have proposed a parameterization of 2D turbulence in the form of a relaxation equation for the coarse-grained PV $\overline{q}(\mathbf{r},t)$. This parameterization is based on a Maximum Entropy Production Principle (MEPP). The diffusion current (due to turbulent mixing) is assumed to maximize the rate of entropy production $\dot{S}$ while conserving all the constraints imposed by the dynamics. In the two-levels case, this yields a system of equations of the form

$$\frac{\partial\overline{q}}{\partial t} + \mathbf{u}\cdot\nabla\overline{q} = \nabla\cdot[D\,(\nabla\overline{q} + \beta(t)(a_1-\overline{q})(\overline{q}-a_{-1})\nabla\psi)], \qquad (142)$$

$$\beta(t) = -\frac{\int D\nabla\overline{q}\cdot\nabla\psi\,d\mathbf{r}}{\int D(a_1-\overline{q})(\overline{q}-a_{-1})(\nabla\psi)^2\,d\mathbf{r}}, \quad (143)$$

$$q = -\Delta\psi + \frac{\psi}{R^2} - Rh(y). \qquad (144)$$

Interestingly, these drift-diffusion equations are similar to the regularized chemotactic model (19–20) introduced in this paper. In this analogy, the coarse-grained PV $\overline{q}$ plays the role of the bacterial concentration and the stream function ψ the role of the chemical c. The analogy between biological aggregates (chemotaxis) and 2D vortices (geophysical turbulence) was noted in [5,18,20]. An important difference, however, is that in 2D turbulence the energy is conserved so that the inverse temperature $\beta(t)$ evolves in time. By contrast, in the chemotactic problem, we are in a situation where the "effective temperature" $T_{eff} = 1/\beta$ is fixed. Therefore, 2D turbulence corresponds to a microcanonical situation (where we maximize the entropy S at fixed energy E) while chemotaxis corresponds to a canonical situation (where we minimize an effective free energy $F = E - T_{eff}S$). These two situations are considered in [18]. For long-range interactions ($k = 0$ or $R \to +\infty$), the "statistical ensembles" (microcanonical vs canonical) are generically inequivalent. However, for short-range interactions ($k \to +\infty$ or $R \to 0$), they become equivalent.

The equilibrium problem (141–144) has been studied in the limit of small Rossby radius $R \to 0$. The original idea dates back to Sommeria et al. [28] who understood that, in this limit, the solution is made of two uniform PV regions separated by a strong jet. This model has been developed quantitatively by Bouchet and Sommeria [29] with comparison to jovian data. Our study of the regularized chemotactic problem has been directly inspired by these works. In complement, we have provided in Section 3 a detailed study of the wall equation with useful asymptotic expansions and analytical approximations. Due to the analogy between the two problems, our results can also be relevant to describe the jet structure of jovian vortices, like GRS. In this respect, we recall that the GRS corresponds to a typical parameter u in the range $0.92 \le u \le 1$ [29] so that the limit $u \to 1$ or $T \to 0$ of our study (Sects. 3.5, 3.7 and 3.8) is particularly interesting in that respect. To strengthen the comparison between the two problems (chemotaxis and jovian vortices), we briefly recall the main lines of the study of Bouchet and Sommeria [29] and provide some complementary discussion.

4.3 Domain wall theory of Jupiter's great red spot

4.3.1 The jet equation

Combining equations (144) and (141), we find that the streamfunction satisfies the meanfield equation

$$-\Delta\psi + \frac{\psi}{R^2} - Rh(y) = B - \tanh\left(\alpha - \frac{C\psi}{R^2}\right). \quad (145)$$

We shall solve this equation perturbatively as an expansion in powers of R. We only give the main lines and refer to Bouchet and Sommeria [29] for more details and developements. To first order, we obtain the jet equation

$$-\frac{d^2\psi}{d\xi^2} - \frac{1}{r}\frac{d\psi}{d\xi} + \frac{\psi}{R^2} - Rh(y) = B - \tanh\left(\alpha - \frac{C\psi}{R^2}\right), \qquad (146)$$

where r is the curvature radius. Introducing the notations

$$\tau = \xi/R, \qquad \phi = \frac{\psi}{R^2} - \frac{\alpha}{C}, \qquad (147)$$

we get

$$\frac{d^2\phi}{d\tau^2} + \frac{R}{r}\frac{d\phi}{d\tau} + Rh(y) = -\tanh(C\phi) + \phi + \frac{\alpha}{C} - B. \qquad (148)$$

To leading order in $R \ll 1$, the foregoing equation reduces to

$$\frac{d^2\phi}{d\tau^2} = -\tanh(C\phi) + \phi + \frac{\alpha_0}{C} - B. \qquad (149)$$

The condition of solvability (see Sect. 3.2) implies that $\alpha_0 = CB$ so that the jet equation takes the form

$$\frac{d^2\phi}{d\tau^2} = -\tanh(C\phi) + \phi = -U'(\phi). \qquad (150)$$

This is the same equation as equation (67) with $C = 1/T$. In the present context, ϕ is related to the streamfunction and $v = d\phi/d\tau$ to the jet velocity. Therefore, the figures representing the profile of concentration gradient in Section 3 give the jet velocity profile in the present context. The PV and streamfunction in the two phases are

$$q_\pm = \frac{\psi_\pm}{R^2} = B \pm u. \qquad (151)$$

Using $\langle q \rangle = 0$, their area is given by

$$A_\pm = \frac{1}{2}\left(1 \mp \frac{B}{u}\right), \qquad (152)$$

which is similar to equation (134). Finally, in the present context, the parameter u is determined by the energy according to the relation

$$E = \frac{1}{2}R^2(u^2 - B^2), \qquad (153)$$

obtained from equations (140, 151) and (152). The series of equilibria $\beta(E)$ is represented in Figure 18. It is univalued confirming that the ensembles are equivalent.

4.3.2 The underlying shear

To first order in R, the jet equation becomes

$$\frac{d^2\phi}{d\tau^2} + \frac{R}{r}\frac{d\phi}{d\tau} + Rh(y) = -U'(\phi) + R\alpha_1, \qquad (154)$$

where we have written $\alpha = \alpha_0 + R\alpha_1 + ...$ and used the fact that $\alpha_0 = CB$. Far from the jet where $\phi \to u$, we can neglect the derivatives so that

$$Rh(y) = -U'(\phi) + R\alpha_1. \qquad (155)$$

Writing $\phi = u + R\delta\phi$ where $\delta\phi$ is a small perturbation, we get to first order $\delta\phi = (\alpha_1 - h(y))/U''(u)$. Therefore, the velocity of the shear around the vortex $\mathbf{v}_{shear} = \delta\phi'(y)\mathbf{e}_x$ is given by

$$v_{shear} = \frac{h'(y)}{-U''(u)} = \frac{h'(y)}{1 - C(1-u^2)}. \qquad (156)$$

Now, the analysis of the jet equation in Section 3.3 shows that the function appearing in the denominator of equation (156) is related to the jet width (78). Therefore, we get the relatively compact equation for the shear velocity

$$v_{shear}(y) = \frac{1}{4}h'(y)L(u)^2, \qquad (157)$$

expressed in terms of the topography and jet width. This relation completes the analysis of [29].

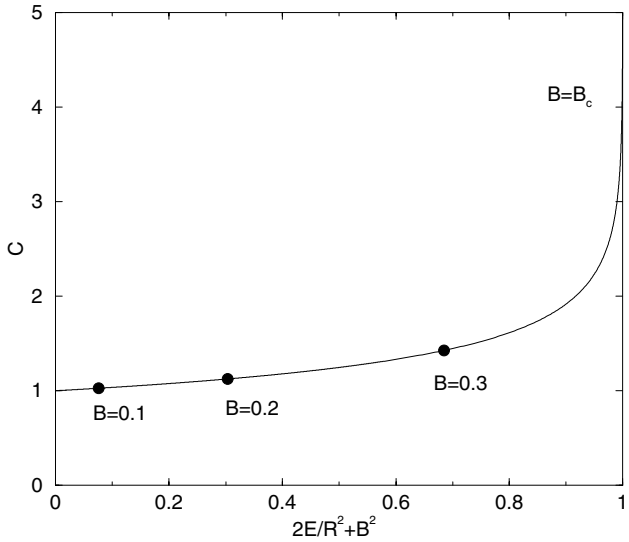

Fig. 18. Caloric curve giving the inverse temperature C as a function of the energy E for jovian vortices in the limit of small radius of deformation $R \to 0$. This curve is obtained from equations (153)-(69) in the absence of topography. In terms of the variable $2E/R^2 + B^2$, this curve is independent on B. We have indicated by a 'bullet' the point of bifurcation (corresponding to $u = \pi B/(\pi - 2)$; see Sect. 3.11) between a vortex (spot, left) and a straight jet (stripe, right), for different values of B: 0.1, 0.2 and 0.3.

4.3.3 The curvature-topography relation

Finally, multiplying equation (154) by $d\phi/d\tau$ and integrating accross the jet, we obtain

$$\frac{e(u)}{r} = u(h(y) - \alpha_1), \qquad (158)$$

which relates the radius of curvature r to the underlying topography $h(y)$. For a given topography, equation (158) determines the form of the jet. This problem has been studied in detail in Bouchet and Sommeria [29] in the case of a quadratic topography. As another example, we consider here the inverse problem: given the form of the jet, find the corresponding topography. We consider the case of an elliptical vortex (see Fig. 19) because this is a relatively good representation of Jupiter's great red spot and we can obtain analytical results in that case.

The topography leading to an elliptic vortex has the form

$$h(y) = \frac{H}{\left[1 + (y/L)^2\right]^{3/2}}, \qquad (159)$$

where L and H are typical horizontal and vertical length scales. Assuming that this relation holds for $|y| \to +\infty$, we must take $\alpha_1 = 0$ in equation (158) to have a vanishing curvature at infinity where $h \to 0$. Therefore, the curvature radius of the vortex is given by

$$\frac{L\chi}{r} = \left[1 + (y/L)^2\right]^{-3/2}, \qquad (160)$$

where we have defined $\chi = e(u)/uHL$. This is the equation of an ellipse with major and minor semi-axis:

$$a = \frac{L\chi}{1-\chi^2}, \quad b = \frac{L\chi}{\sqrt{1-\chi^2}}. \tag{161}$$

These relations assume that $\chi \leq 1$. Now, in the case of GRS, the aspect ratio

$$\frac{a}{b} = \frac{1}{\sqrt{1-\chi^2}}, \tag{162}$$

is close to 2 leading to $\chi = \sqrt{3}/2$. The major and minor semi-axis are then given by $a = 2\sqrt{3}L$ and $b = \sqrt{3}L$.

Consider now the limit $\chi \to 0$. In that case, the width of the vortex is small with respect to the horizontal topographic length ($b \ll L$) and we can make the quadratic approximation

$$h(y) \simeq H - \frac{3}{2}\frac{H}{L^2}y^2. \tag{163}$$

This is similar to the situation considered by Bouchet and Sommeria [29]. Their parameter d is related to our parameter χ by $d = (3/2)\chi^2$. For a quadratic topography with $(\chi, d) \to 0$, our study shows that the vortex shape is an ellipse whose major and minor semi-axis are given by equations (161). In particular, the aspect ratio behaves like

$$\frac{a}{b} = 1 + \frac{d}{3} + ... \qquad (d \to 0). \tag{164}$$

However, this formula is not applicable for a vortex with aspect ratio $\sim$2 like GRS. In their approach, Bouchet and Sommeria [29] assume a quadratic topography and solve the curvature-topography relation numerically. For large values of d, close to its maximal value $d_{max} = 4/9$, the vortex is not an ellipse. Alternatively, if we assume a topography of the form (159) we find an elliptic vortex for all the values of $\chi \leq 1$. This suggests that the form of the vortex is relatively sensitive to the underlying topography.

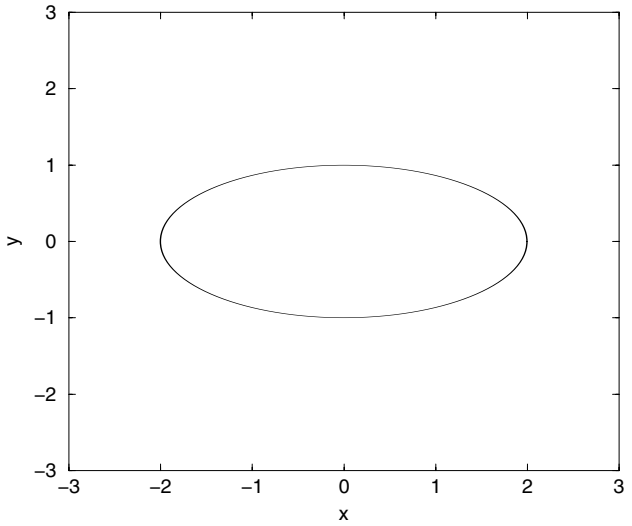

Fig. 19. Elliptic vortex with aspect ratio of 2 above a topography of the form (159). The solid line represents the thin jet separating the two regions with uniform potential vorticity.

5 Connection to other works on chemotaxis

There is a huge literature on the chemotaxis problem in the community of applied mathematics [16]. In this section, we provide a short review of the history of the Keller-Segel model and its generalizations so as to place our contribution in a broader context. The discussion that we provide here and in [5,20] emphasizes the physical results and the connection between chemotaxis, self-gravitating systems, 2D vortices, Bose-Einstein condensation, generalized thermodynamics, Burgers dynamics and Cahn-Hilliard equations which is not developed in other reviews.

5.1 The Keller-Segel model and the formation of Dirac peaks

In seminal papers, Patlak [2] and Keller and Segel [3] introduced a mathematical formulation of the process of chemotactic aggregation. They modeled the interaction between the cellular slime molds (amoebae) and the chemical substance (acrasin) produced by these organisms in terms of the two coupled PDEs (1–2). The mechanism proposed by Keller and Segel [3] for the initiation of cells aggregation is described as a linear instability of the spatially homogeneous equilibria of equations (1–2). Several authors have then studied the nonlinear regime of the aggregation process through the "reduced" Keller-Segel model (3–4) where the diffusion coefficient and the chemotactic sensitivity are constant. Nanjundiah [60] was the first to suggest that the aggregation proceeds to the formation of delta-functions in cell density, a phenomenon later referred to as "chemotactic collapse". This possibility has been studied in detail by Childress and Percus [61], Jäger and Luckhaus [4], Nagai [62], Othmer and Stevens [63] and Biler [64] among others. It is shown that blow-up never occurs in one dimension (unless there is no diffusion of the attractant). In two dimensions, there exists a critical mass M_c such that if $M > M_c$ then blow-up can occur while there is no collapse for $M < M_c$. In three or more dimensions, blow-up can occur even for small masses M.

To simplify the problem, Jäger and Luckhaus [4] considered a limit of high diffusivity of the chemical and showed that equation (4) is then replaced by $\Delta c = -\lambda(\rho - \overline{\rho})$ where $\lambda = a/D'$ and $\overline{\rho} = \frac{1}{V}\int \rho d\mathbf{r}$ denotes the average value of the density over the domain. In the collapse regime where $\rho \gg \overline{\rho}$, this relation reduces to a Poisson equation $\Delta c = -\lambda\rho$. The simplified Keller-Segel model obtained by coupling equation (3) to this Poisson equation has been studied by different authors. Herrero and Velazquez [65] considered the problem in $d = 2$ and showed, using matched asymptotic expansions, that for $M > M_c$ the system collapses to a Dirac peak in a finite time. Herrero et al. [66] considered the problem in $d = 3$ and constructed a (non self-similar) solution consisting of an imploding, smoothed-out, shock that collapses

into a Dirac mass when the singularity is formed. Herrero et al. [67] and Brenner et al. [68] constructed self-similar solutions of the chemotactic collapse in $d = 3$. However, these solutions do *not* lead to a concentration of mass (Dirac peak) at the origin.

Independently, Chavanis and Sire [6–14] introduced and systematically studied the dynamics and the thermodynamics of a system of self-gravitating Brownian particles. They considered a mean-field approximation (which is exact in a properly defined thermodynamic limit $N \to +\infty$ with $\Lambda = -ER^{d-2}/GM^2$ and $\eta = \beta GMm/R^{d-2}$ fixed [30,31]) and a strong friction regime $\xi \to +\infty$ where the dynamics reduces to the study of the Smoluchowski-Poisson system. In the course of their study, they realized that the Smoluchowski-Poisson system was isomorphic to the simplified version of the Keller-Segel model described above so that their results apply equally well to biological populations by a proper re-interpretation of the parameters [5]. They also showed the analogy with the Bose-Einstein condensation in the canonical ensemble [19,20] and with the statistical mechanics of two-dimensional vortices [5,20]. In [6,7], they studied the structure and the stability of equilibrium solutions of the Smoluchowski-Poisson system confined within a box (corresponding to isothermal self-gravitating spheres) and showed that, in $d \geq 2$, these solutions exist only above a critical temperature T_c. For $T < T_c$, there is no steady state and the system undergoes an isothermal collapse. In $d > 2$, they constructed analytically self-similar collapse solutions that lead to a finite time singularity (the density profile behaves like $\rho \propto 1/r^2$ at $t = t_{coll}$). This self-similar collapse [6,7] does not lead to a concentration of mass at the origin (Dirac peak) but it was shown in [9] that a Dirac peak is formed in the *post-collapse* regime of the dynamics, after the singularity has arisen. The dependence of the collapse time $t_{coll} \sim (T_c - T)^{-1/2}$ with the distance to the critical temperature was obtained analytically in [10]. Since the self-similar solutions are expected to describe the collapse below the critical temperature T_c, the collapse time diverges when $T \to T_c^-$ indicating the existence of a stable gaseous phase above T_c. Indeed, for $T > T_c$, it is found numerically [6] that, under normal circumstances, the system tends to an equilibrium state. Collapse can also occur above T_c but this demands very particular initial conditions. These two possible regimes (collapse or convergence to an equilibrium state) arise because the gaseous equilibrium solutions are only *local* minima of free energy (long-lived metastable states) while the collapse solutions ultimately lead to Dirac peaks with infinite free energy (global minima of free energy) [7]. The choice between these two regimes then depends on a complicated notion of *basin of attraction* [6]. In $d = 2$, it is shown in [7] that collapse occurs below a critical temperature T_c and leads to a Dirac peak containing a fraction T/T_c of the total mass surrounded by a density profile (halo) evolving almost self-similarly[2]. From the Virial theorem [13], it can be shown that the Dirac peak accretes the rest of the mass in the post-collapse regime. At $T = T_c$, the evolution is self-similar and a Dirac peak containing the whole mass is formed in infinite time. In a bounded domain, the central density increases exponentially with time [7]. For $T > T_c$, the system reaches an equilibrium state which is a global minimum of free energy. In $d = 1$, there is no collapse (except at $T = 0$) and the evolution of the mass profile satisfies a Burgers equation. The case of an unbounded domain has been studied by Chavanis and Sire [13,14]. For $d > 2$, they showed that the system can either collapse (like in a box) or undergo a diffusion process (evaporation). They determined the correction to pure diffusion due to the gravitational attraction and showed that self-gravity becomes negligible for large times. For $d = 2$, they determined the exact diffusion coefficient of the self-gravitating Brownian gas. This diffusion coefficient becomes negative below the critical temperature T_c leading to the formation, in a finite time, of a Dirac peak containing the whole mass. At $T = T_c$, the Dirac peak is formed in infinite time and the central density increases logarithmically [13] with time instead of exponentially [7] in a bounded domain. A tiny amount of mass is ejected at large distances so as to satisfy the conservation of the moment of inertia. For $T > T_c$, the system evaporates. This process is self-similar and it has been studied analytically [13] for $T \gg T_c$ and $T \to T_c^+$. For $d = 1$, the system reaches an equilibrium state.

5.2 Many-body models of chemotaxis and statistical fluctuations

The Keller-Segel model (3–4) is a continuous model where the evolution of the distribution of cells is described by a smooth density field. Several authors have tried to derive this model from a more microscopic approach (N-body system) to better determine its domain of validity.

Schweitzer and Schimansky-Geier [69] introduced a stochastic model of Brownian particles in interaction that they called active walkers. The walkers are able to change locally the potential in which they move by producing a second component B. The nonlinear feedback between the density distribution of both components results in a clustering of the walkers. Schweitzer and Schimansky-Geier [69] studied their agglomeration on a two-dimensional surface. Their description is based on a set of Langevin and Fokker-Planck equation for the active walkers, coupled by a reaction-diffusion equation for the component B. The Fokker-Planck equation, obtained in a mean-field approximation (which is not rigorously justified in their work), is similar to the Keller-Segel model. Apparently, these authors were not aware of that model

[2] With the notations of biology appropriate to the Keller-Segel model, this solution corresponds to the formation of a Dirac peak containing a mass M_c (the critical mass in $d = 2$) surrounded by a density profile evolving almost self-similarly. This solution, vindicated by direct numerical simulations of the Smoluchowski-Poisson system [7], is different from the one given by Herrero and Velazquez [65]. The reason for this discrepancy is not well understood but it is possible that the solution of [65] is unstable.

since it is not referenced. They made contact, however, to the general process of chemotaxis in biology.

Stevens [70] rigorously derived the PDEs of the Keller-Segel model from an interacting stochastic many-particles system, where the interaction between the particles is rescaled in a moderate way as population size tends to infinity.

Newman and Griman [71] developed a many-body theory of cell-cell interactions. They used methods of statistical physics and field theory and derived an exact kinetic equation for the one-body probability distribution involving the two-body distribution. In the mean-field limit, where statistical correlations between cells are neglected, the deterministic Keller-Segel equations (3, 4) are recovered. They also took into account statistical correlations and described them by a perturbation theory in the limit of weak coupling. This leads to a renormalization of the cell diffusion coefficient. Following this work, Grima [72] introduced a non-perturbative approach to compute the diffusion coefficient and discussed the similarities and the differences between the stochastic models and their deterministic (mean field) counterparts.

Chavanis [30,31] (see also [5,14,32]) studied stochastic models of Brownian particles coupled by a weak long-range binary potential of interaction. Such models describe in particular self-gravitating Brownian particles and biological populations (in simplified settings). Both inertial and overdamped systems are treated while other studies consider a strong friction limit $\xi \to +\infty$ (or a limit of large times $t \gg \xi^{-1}$). A hierarchy of kinetic equations for the reduced probability distributions is derived in [31] and the mean-field Kramers and mean-field Smoluchowski equations are obtained in the large N limit where the correlations are found to become negligible (the proper thermodynamic limit corresponds to $N \to +\infty$ in such a way that the coupling constant $k \sim 1/N$ with energy $E \sim N$, temperature $T \sim 1$ and volume $V \sim 1$). For a Newtonian potential of interaction, this leads to the Smoluchowski-Poisson system describing self-gravitating Brownian particles. This also corresponds to the simplified version of the Keller-Segel model describing biological populations. This study shows that the mean-field approximation provides a very good description of systems with long-range interactions, provided that N is sufficiently large (it becomes exact in the thermodynamic limit $N \to +\infty$ defined above).

5.3 The regularized Keller-Segel model and the formation of smooth aggregates

The "reduced" Keller-Segel model (3–4) ultimately leads to the formation of Dirac peaks. Since these singularities are unphysical, several authors have introduced regularized versions of the Keller-Segel model where the Dirac peaks are replaced by smooth aggregates with bounded density. These regularized models are particular cases of the "primitive" Keller-Segel model (1–2).

Hillen and Painter [73] studied a version of the Keller-Segel model where the chemotactic sensitivity depends on both the external signal and the local population density. In the case where the chemotactic response is switched off at high cell densities (due to volume filling) they showed that there is no finite time blow-up of the solutions but rather formation of stable aggregates. They could prove therefore local and global existence in time of classical solutions. Painter and Hillen [74] pursued their investigation and derived the Keller-Segel equation from a master equation for a continuous-time discrete-space random walk on a one-dimensional lattice. The model where the chemotactic sensitivity depends on the local population density is obtained by allowing the probability of jumping into neighbouring sites to depend on the amount of space available at that site. They performed numerical simulations showing the formation of aggregates that progressively merge until only one structure remains at the end.

Independently, in the context of generalized thermodynamics pioneered by Tsallis [75], some authors have introduced a class of nonlinear Fokker-Planck equations associated with non-standard equilibrium distributions [18, 36,76,77]. These equations can be obtained from usual Fokker-Planck equations by allowing the diffusion coefficient and the friction force (or the mobility for overdamped models) to depend on the concentration of particles. Chavanis [18] considered situations where these generalized Fokker-Planck equations are furthermore coupled to a mean-field potential and mentioned applications to chemotaxis. Indeed, the regularized Keller-Segel model (19–20) where the chemotactic sensitivity depends on the local population density appears to be a special class of these general equations (we can also consider models where the diffusion coefficient depends on the density as in [8,78]). These nonlinear Fokker-Planck equations have a generalized thermodynamical structure [18]. They can be derived from a generalized class of stochastic equations [18] or from a master equation by allowing the probability of transition to depend on the concentration in the initial and arrival sites [36]. This is equivalent to the arguments of Painter and Hillen [74]. Therefore, the derivation of the regularized model given in Section 2.3 can be viewed as an alternative to the one given by Painter and Hillen [74]. The particular case where the chemotactic sensitivity is proportional to $\rho(1-\rho/\sigma_0)$ was proposed in [5,18] on the basis of phenomenological arguments, as a simple regularization of the Keller-Segel model preventing blow-up. Using an analogy with self-gravitating fermions and two-dimensional vortices [26,79], it was argued in [5] that the density remains always bounded by σ_0 (this is obvious at equilibrium) so that this model leads to stable aggregates instead of Dirac peaks. With such a regularization, the dynamics of the Keller-Segel model is similar to a coarsening dynamics in phase ordering kinetics [17]. Indeed, starting from a random initial condition, domains (aggregates) spontaneously form and grow until only one big structure remains. This analogy can be made more precise by noting (see [22]) that, in the limit of short-range interactions, the Keller-Segel model can be put in a form similar to the Cahn-Hilliard equation. In fact, the

Keller-Segel model can be viewed as a generalization of the Cahn-Hilliard equation to the case of systems with long-range interactions.

Finally, in a recent work, Holm and Putkaradze [80,81] considered a drift-diffusion model[3] where the mobility of the particles depends on the configuration of their neighbors and linear diffusion acts on locally averaged particle density $\overline{\rho}$. In the absence of diffusion ($D = 0$), they showed that Dirac peaks (clumpons) emerge from smooth initial conditions and that the evolution of these clumpons is governed by a system of N differential equations. When the mobility vanishes for some averaged density $\overline{\rho}_*$, the clumpons are replaced by jammed patches (a weak solution with the density having compact support). Holm and Putkaradze [81] constructed stationary solutions of their model in which the density forms a plateau with $\rho = \overline{\rho}_*$ in the core and $\rho = 0$ outside. They showed that the interface can have several shapes: stripes, circles, ellipses, parabolae and hyperbolae. This type of solutions where the core density reaches its maximum value $\overline{\rho}_*$ corresponds to the zero temperature limit of our model. In that case, the Fermi-Dirac distribution (21) reduces to the Heaviside function where ρ passes from σ_0 to 0. In this $T = 0$ limit, it is possible to construct analytical solutions of equations (21–20) for arbitrary value of the screening length k^{-1}. Various frontier shapes can be obtained in agreement with the results of Holm and Putkaradze [81]. This is not in contradiction with the results of the present study where we consider another limit. Indeed, we treat arbitrary values of the temperature (or diffusion coefficient D) but we focus on short range interactions where $k \to +\infty$. In that case, the steady states exhibit a density plateau with $\rho = \rho_{max} < \sigma_0$ in the core and $\rho = \rho_{min} > 0$ outside. Then, minimization of free energy (see Sect. 3.10) implies that the interface must be either a stripe or a circle.

[3] In their "Historical perspective of continuum models of self-aggregation" (Sect. 1), Holm and Putkaradze [81] attribute the study of the Smoluchowski-Poisson system to Chandrasekhar [82], although Chandrasekhar never considered the coupling between the Smoluchowski and the Poisson equations. In his classical work on stellar dynamics, Chandrasekhar studied the relaxation of a test star in a *thermal bath* of field stars with frozen distribution function, by developing an analogy with Brownian theory [83]. This leads to the Kramers equation with a *fixed external* potential $\Phi(\mathbf{r})$. Chandrasekhar furthermore assumed that the distribution of the field stars is infinite and homogeneous (so that $\Phi = 0$) and used the Kramers equation to determine the rate of escape of stars from a globular cluster. It would be tempting to describe the dynamical evolution of the stellar system "as a whole" by the Kramers-Poisson or Smoluchowski-Poisson equations (see comments of Chandrasekhar [83] in Sect. 4.). However, these equations *cannot* rigorously describe a stellar system, which has a Hamiltonian structure, since they do not conserve energy. This is probably why these equations have never been considered in astrophysics. The correct kinetic equation for a stellar system is the Landau-Poisson system [84,85] which conserves energy and which is therefore appropriate to a Hamiltonian system described by the microcanonical ensemble. The Kramers-Poisson and Smoluchowski-Poisson equations have been introduced in [6–14] for a self-gravitating Brownian gas, not a stellar system, which is described by the canonical ensemble where the temperature is fixed. The distinction between the kinetic theory of Hamiltonian and Brownian systems of particles with long-range interactions is further discussed in [30,31].

6 Conclusion

In this paper, we have studied the equilibrium states of a regularized version of the Keller-Segel model describing the chemotactic aggregation of bacterial colonies. The regularization is justified physically in order to avoid the formation of singularities (Dirac peaks) during the dynamics and obtain smooth density profiles (aggregates) instead. This regularization accounts for finite size effects and close packing effects. In that case, an equilibrium state exists for any value of the control parameter contrary to the usual Keller-Segel model leading to blow-up (this is similar to considering a gas of self-gravitating fermions in astrophysics to avoid singularities corresponding to complete gravitational collapse [79]). We have studied furthermore a limit of high degradation of the chemical $k \to +\infty$. In previous works [6–14], the opposite limit $k = 0$ (no degradation) was considered instead. The intermediate case of a finite degradation rate, which is certainly the case of most physical interest, must be studied numerically (in preparation). However, the asymptotic limit $k \to +\infty$ allows us to obtain analytical results that permit to have a clear picture of the bifurcation diagram (between spots and stripes) in parameter space. Furthermore, our approach is exact in one dimension, for any value of the degradation rate k. Our study shows that the physics of the problem is sensibly different whether $k \ll 1$ or $k \gg 1$.

We have also discussed the analogy between the organization of bacteria (in stripes and spots) in the chemotactic problem and the organization of two-dimensional turbulent flows (in jets and vortices) in the jovian atmosphere. These apparently completely different systems are described by relatively similar equations so that an interesting analogy can be developed between them. In this analogy, the jet structure of Jupiter's great red spot can be seen as a 'domain wall' that is similar to the interface separating two phases in contact, as in the biological problem when $k \gg 1$.

We would like to conclude this paper on some possible applications of our results in biology. Models of chemotaxis have been successfully applied to many systems, including aggregation patterns in bacteria [87–89], fish skin pigmentation patterns [90], angiogenesis in tumour progression and wound healing [91–93], and many other examples. In particular, bacteria such as *E. coli* have been shown to form a range of patterns such as rings and spots. The shapes of these structures are consistent with those found in the present study. Other examples of application are given by Painter and Hillen [74]. Network patterns have also been observed in recent experiments of in vitro formation in blood vessels. They are interpreted as the beginning of a vasculature, a phenomenon responsible

of angiogenesis, a major actor for the growth of tumors. However, these connected vascular networks cannot be explained by parabolic models of the Keller-Segel type. They are explained in general in terms of hyperbolic models (similar to hydrodynamic equations) [86,94]. The mathematical study of these chemotactic models can shed light on the diversity of patterns observed in biology. These biophysical structures, together with galaxies in astrophysics and vortices in two-dimensional turbulent flows [21], are striking examples of self-organization in nonlinear media, due to the long-range attraction of a potential of interaction.

Appendix A: Stability analysis

We study the linear dynamical stability of an infinite and homogeneous solution of the regularized Keller-Segel model (19–20). The unperturbed solution satisfies

$$k^2 c = \lambda\rho. \tag{165}$$

Linearizing equations (19, 20) around this steady state and writing the perturbation as $\delta\rho = \delta\hat{\rho}e^{i\mathbf{q}\cdot\mathbf{r}}e^{\sigma t}$, $\delta c = \delta\hat{c}e^{i\mathbf{q}\cdot\mathbf{r}}e^{\sigma t}$, we obtain

$$\chi\rho(1-\rho/\sigma_0)q^2\delta\hat{c} - (Dq^2+\sigma)\delta\hat{\rho} = 0, \tag{166}$$

$$(q^2+k^2)\delta\hat{c} - \lambda\delta\hat{\rho} = 0. \tag{167}$$

This system of equations admits non-trivial solutions only if the determinant is zero yielding the dispersion relation

$$\sigma = q^2\left(\frac{\chi\lambda\rho(1-\rho/\sigma_0)}{q^2+k^2} - D\right). \tag{168}$$

The system is unstable if $\sigma > 0$ and stable otherwise. A necessary condition of instability is

$$\frac{\chi}{D}\lambda\rho(1-\rho/\sigma_0) - k^2 \geq 0. \tag{169}$$

If this condition is fulfilled, the unstable wavenumbers are

$$q^2 \leq \frac{\chi}{D}\lambda\rho(1-\rho\sigma_0) - k^2 \equiv q_{max}^2. \tag{170}$$

For $u = 0$, i.e. $\rho = \sigma_0/2$ (see Sect. 3), we find that the instability criterion (169) corresponds to

$$T \leq T_c = 1. \tag{171}$$

Therefore, the uniform phase $u = 0$ is stable for $T > T_c$ and unstable for $T < T_c$ where it is replaced by a 'stripe' or a 'spot' formed in the nonlinear regime (see Fig. 2). The unstable wavenumbers are

$$q^2 \leq (C-1)k^2 \equiv q_{max}^2, \tag{172}$$

where we recall that $C = 1/T$. The growth rate (see Fig. A.1) can be written

$$\sigma = Dq^2\left(\frac{Ck^2}{q^2+k^2} - 1\right). \tag{173}$$

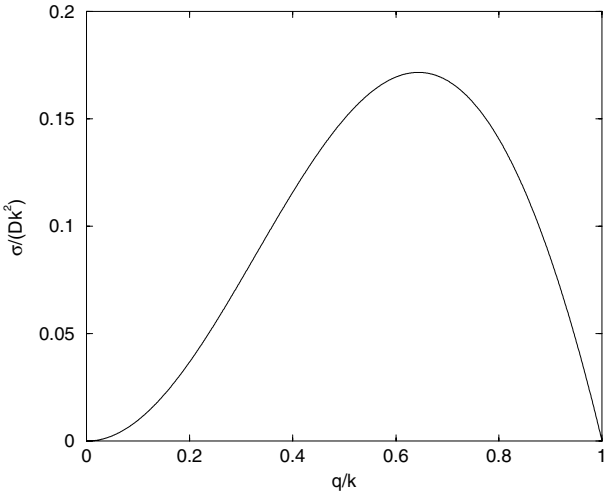

Fig. A.1. Growth rate of the perturbation as a function of the wavenumber for $T = 1/2 < T_c$.

The maximum growth rate is obtained for

$$q_*^2 = k^2(\sqrt{C}-1), \tag{174}$$

and its value is

$$\sigma_* = Dk^2(\sqrt{C}-1)^2. \tag{175}$$

A more general linear dynamical stability analysis of the Keller-Segel model (and generalizations) is performed in [86].

Appendix B: Surface tension for $T \to 0$

Using equations (81) and (73), the surface tension can be written

$$\sigma = 2\int_0^u (\phi^2 - 2T\ln[\cosh(\phi/T)] - u^2 + 2T\ln[\cosh(u/T)])^{1/2}d\phi. \tag{176}$$

Using

$$\ln[\cosh(\phi/T)] = \phi/T - \ln 2 + \ln(1+e^{-2\phi/T}), \tag{177}$$

and considering the limit $T \to 0$, we obtain

$$\sigma = 2\int_0^1 \sqrt{(1-\phi)^2 - 2T\ln(1-e^{-2/T}+e^{-2\phi/T})}d\phi. \tag{178}$$

Setting $x = 1-\phi$, this can be rewritten

$$\sigma = 2\int_0^1 x\sqrt{1 - \frac{2T}{x^2}\ln\left[1+e^{-2/T}(e^{2x/T}-1)\right]}dx. \tag{179}$$

For $T \to 0$, we obtain

$$\sigma = 2 \int_0^1 x \left(1 - \frac{T}{x^2} \ln \left[1 + e^{-2/T} (e^{2x/T} - 1) \right] \right) dx. \tag{180}$$

Setting $y = 2x/T$, we find that

$$\sigma = 1 - 2T \int_0^{2/T} \ln \left[1 + e^{-2/T} (e^{y} - 1) \right] \frac{dy}{y}. \tag{181}$$

Setting $x = 2/T - y$, we get

$$\sigma = 1 - 2T \int_0^{2/T} \ln \left[1 + e^{-2/T} (e^{2/T - x} - 1) \right] \frac{dx}{2/T - x}. \tag{182}$$

For $T \to 0$, we finally obtain

$$\sigma = 1 - T^2 \int_0^{+\infty} \ln \left(1 + e^{-x} \right) dx. \tag{183}$$

Using

$$\int_0^{+\infty} \ln \left(1 + e^{-x} \right) dx = \frac{\pi^2}{12}, \tag{184}$$

we establish equation (97).

References

1. J.D. Murray, *Mathematical Biology* (Springer, Berlin, 1991)
2. C.S. Patlak, Bull. of Math. Biophys. **15**, 311 (1953)
3. E.F. Keller, L.A. Segel, J. Theor. Biol. **30**, 225 (1971)
4. W. Jäger, S. Luckhaus, Trans. Amer. Math. Soc. **329**, 819 (1992)
5. P.H. Chavanis, M. Ribot, C. Rosier, C. Sire, Banach Center Publ. **66**, 103 (2004)
6. P.H. Chavanis, C. Rosier, C. Sire, Phys. Rev. E **66**, 036105 (2002)
7. C. Sire, P.H. Chavanis, Phys. Rev. E **66**, 046133 (2002)
8. P.H. Chavanis, C. Sire, Phys. Rev. E **69**, 016116 (2004)
9. C. Sire, P.H. Chavanis, Phys. Rev. E **69**, 066109 (2004)
10. P.H. Chavanis, C. Sire, Phys. Rev. E **70**, 026115 (2004)
11. C. Sire, P.H. Chavanis, Banach Center Publ. **66**, 287 (2004)
12. J. Sopik, C. Sire, P.H. Chavanis, Phys. Rev. E **72**, 026105 (2005)
13. P.H. Chavanis, C. Sire, Phys. Rev. E **73**, 066103 (2006)
14. P.H. Chavanis, C. Sire, Phys. Rev. E **73**, 066104 (2006)
15. P.H. Chavanis, preprint
16. D. Horstmann, Jahresberichte der DMV **106**, 51 (2004)
17. A. Bray, Adv. Phys. **43**, 357 (1994)
18. P.H. Chavanis, Phys. Rev. E **68**, 036108 (2003)
19. J. Sopik, C. Sire, P.H. Chavanis, Phys. Rev. E **74**, 011112 (2006)
20. P.H. Chavanis, C. R. Physique **7**, 318 (2006)
21. P.H. Chavanis, in *Dynamics and thermodynamics of systems with long range interactions*, edited by T. Dauxois, S. Ruffo, E. Arimondo, M. Wilkens, Lecture Notes in Physics (Springer, 2002), e-print `arXiv:cond-mat/0212223`
22. P.H. Chavanis, P. Laurençot, M. Lemou, Physica A **341**, 145 (2004)
23. D. Lynden-Bell, Mon. Not. Roy. Astr. Soc. **136**, 101 (1967)
24. J. Miller, Phys. Rev. Lett. **65**, 2137 (1990)
25. R. Robert, J. Sommeria, J. Fluid Mech. **229**, 291 (1991)
26. P.H. Chavanis, J. Sommeria, R. Robert, Astrophys. J. **471**, 385 (1996)
27. J. Pedlosky, *Geophysical Fluid Dynamics* (Springer, Berlin, 1987)
28. J. Sommeria, C. Nore, T. Dumont, R. Robert, C. R. Acad. Sci. Ser. II **312**, 999 (1991)
29. F. Bouchet, J. Sommeria, J. Fluid Mech. **464**, 165 (2002)
30. P.H. Chavanis, Physica A **361**, 55 (2006)
31. P.H. Chavanis, Physica A **361**, 81 (2006)
32. P.H. Chavanis, preprint
33. P.H. Chavanis, Banach Center Publ. **66**, 79 (2004)
34. P.H. Chavanis, Physica A **332**, 89 (2004)
35. P.H. Chavanis, Physica A **340**, 57 (2004)
36. G. Kaniadakis, Physica A **296**, 405 (2001)
37. J.W. Cahn, J.E. Hilliard, J. Chem. Phys. **28**, 258 (1958)
38. C. Sire, P.H. Chavanis, Phys. Rev. E **61**, 6644 (2000)
39. T.E. Dowling, Annu. Rev. Fluid Mech. **27**, 293 (1995)
40. P.L. Read, R. Hide, Nature **308**, 45 (1984)
41. S. Antipov, M. Nezlin, E. Snezhkin, A. Trubnikov, Nature **323**, 238 (1986)
42. J. Sommeria, S. Meyers, H. Swinney, Nature **331**, 689 (1988)
43. P.S. Marcus, Annu. Rev. Astron. Astrophys. **31**, 523 (1993)
44. T. Maxworthy, L. Redekopp, Icarus **29**, 261 (1976)
45. R. Kraichnan, D. Montgomery, Rep. Prog. Phys. **43**, 547 (1980)
46. A.P. Ingersol, P.G. Cuong, J. Atmos. Sci. **38**, 2067 (1981)
47. G.P. Williams, Adv. Geophys. **28**, 381 (1985)
48. L. Onsager, Nuovo Cimento Suppl. **6**, 279 (1949)
49. G. Joyce, D. Montgomery, J. Plasma. Phys. **10**, 107 (1973)
50. T.S. Lundgren, Y.B. Pointin, J. Stat. Phys. **17**, 323 (1977)
51. G.A. Kuz'min, in *Structural Turbulence*, edited by M.A. Goldshtik (Acad. Naouk CCCP Novosibirsk, Institute of thermophysics, 1982), pp. 103–114
52. P.H. Chavanis, J. Sommeria, J. Fluid Mech **356**, 259 (1998)
53. J. Miller, P.B. Weichman, M.C. Cross, Phys. Rev. A **45**, 2328 (1992)
54. T.E. Dowling, A.P. Ingersoll, J. Atmos. Sci. **46**, 3256 (1989)
55. P.H. Chavanis, J. Sommeria, Phys. Rev. E **65**, 026302 (2002)
56. F. Bouchet, P.H. Chavanis, J. Sommeria, in preparation
57. B. Turkington, A. Majda, K. Haven, M. Dibattista, PNAS **98**, 12346 (2001)
58. P.H. Chavanis, Physica D **200**, 257 (2005)
59. R. Robert, J. Sommeria, Phys. Rev. Lett. **69**, 2776 (1992)
60. V. Nanjundiah, J. Theoret. Biol. **42**, 63 (1973)
61. S. Childress, J.K. Percus, Math. Biosci. **56**, 217 (1981)
62. T. Nagai, Adv. Math. Sci. Appl. **5**, 581 (1995)
63. H.G. Othmer, A. Stevens, SIAM J. Appl. Math. **57**, 1044 (1997)

64. P. Biler, Adv. Math. Sci. Appl. **8**, 715 (1998)
65. M.A. Herrero, J.L. Velazquez, Math. Ann. **306**, 583 (1996)
66. M.A. Herrero, E. Medina, J.L. Velazquez, Nonlinearity **10**, 1739 (1997)
67. M.A. Herrero, E. Medina, J.L. Velazquez, J. Comput. Appl. Math. **97**, 99 (1998)
68. M.P. Brenner, P. Constantin, L.P. Kadanoff, A. Schenkel, S.C. Venkataramani, Nonlinearity **12**, 1071 (1999)
69. F. Schweitzer, L. Schimansky-Geier, Physica A **206**, 359 (1994)
70. A. Stevens, SIAM J. Appl. Math. **61**, 183 (2000)
71. T.J. Newman, R. Grima, Phys. Rev. E **70**, 051916 (2004)
72. R. Grima, Phys. Rev. Lett. **95**, 128103 (2005)
73. T. Hillen, K. Painter, Adv. Appl. Math. **26**, 280 (2001)
74. K. Painter, T. Hillen, Can. Appl. Math. Q. **10**, 501 (2002)
75. C. Tsallis, J. Stat. Phys. **52**, 479 (1988)
76. A.R. Plastino, A. Plastino, Physica A **222**, 347 (1995)
77. T.D. Frank, *Nonlinear Fokker-Planck Equations: Fundamentals and Applications* (Springer-Verlag, 2005)
78. P.H. Chavanis, C. Sire, Physica A **375**, 140 (2007)
79. P.H. Chavanis, Phys. Rev. E **65**, 056123 (2002)
80. D.D. Holm, V. Putkaradze, Phys. Rev. Lett. **95**, 226106 (2005)
81. D.D. Holm, V. Putkaradze, Physica D **220**, 183 (2006)
82. S. Chandrasekhar, *An Introduction to the Theory of Stellar Structure* (Dover, 1939)
83. S. Chandrasekhar, Astrophys. J. **97**, 263 (1943)
84. H. Kandrup, Phys. Rep. **63**, 1 (1980)
85. P.H. Chavanis, Eur. Phys. J. B **52**, 61 (2006)
86. P.H. Chavanis, Eur. Phys. J. B **52**, 433 (2006)
87. R. Tyson, S.R. Lubkin, P. Roy. Soc. Lond. B. Bio. **266**, 299 (1999)
88. R. Tyson, S.R. Lubkin, J. Math. Biol. **38**, 359 (1999)
89. D. Woodward, R. Tyson, M. Myerscough, J. Murray, E. Budrene, H. Berg, Biophys. J. **68**, 2181 (1995)
90. K. Painter, H. Othmer, P. Maini, Proc. Natl. Acad. Sci. USA **96**, 5549 (1999)
91. H. Byrne, M. Chaplain, Bull. Math. Biol. **57**, 461 (1995)
92. L. Olsen, J. Sherratt, P. Maini, F. Arnold, IMA J. Math. Appl. Med. Biol. **14**, 261 (1997)
93. A. Perumpanani, J. Sherratt, J. Norbury, H. Byrne, Physica D **126**, 145 (1999)
94. A. Gamba, D. Ambrosi, A. Coniglio, A. de Candia, S. di Talia, E. Giraudo, G. Serini, L. Preziosi, F. Bussolino, Phys. Rev. Lett. **90**, 118101 (2003)